Static and Dynamic Behaviour of Additive Manufactured Multi-Material Honeycomb Structure

VIJAYANAND RAJENDRA BOOPATHY

MSc by Research

ASTON UNIVERSITY

JUNE 2019

Aston University

Static and Dynamic Behaviour of Additive Manufactured Multi-Material Honey Comb Structure

Vijayanand Rajendra Boopathy
MSc by Research
2019

ABSTRACT

The degree to which a vehicle protects its occupants from the effect of accidents and lightweight requirements in the automotive industry has drawn the attention of composite materials, which have high specific stiffness, strength and energy absorbing capability. At present bumper design is made of single material which constrains it to the property of that particular material only. Additive manufacturing is a technique, which paves way for the manufacturing the combination of multiple materials. Among these combinations of materials, the main aim of the multi-material honeycomb structure is to resist the motion after impact and at the same time absorb energy progressively. The present study aims in providing new possibilities for combining multiple properties in a single product and investigating the effect of various design for additive manufacturing applications. From the results of dynamic FEA, a progressive failure is observed in the multi-material honeycomb structure with increased absorption of energy than single material. The force increases with increase in cell wall thickness due to the stiffness of the material and the force increases with decrease in cell wall size for both single and multi-material honeycomb structure. From the results of static FEA and static experimentation, a progressive failure is observed in multi-material honeycomb structure with increased absorption of energy than single material. The force increases with increase in cell wall thickness due to the stiffness of the material and the force increases with decrease in cell wall size for both single and multi-material honeycomb structure. From the static experimentation results of multi-material honeycomb structure the cell wall thickness of 1mm in multi-material the force experienced by cell size of 3.5mm is 82.3% lower than the cell size of 2.5mm. For cell wall thickness of 1mm in multi-material the force experienced by cell size of 3mm is 55.6% lower than the cell size of 2.5mm. For cell wall thickness of 1mm in multi-material the force experienced by cell size of 2.5mm is maximum. For cell wall thickness of 1.5 mm in multi-material the force experienced by cell size of 3.5mm is 77.8% lower than the cell size of 2.5mm. For cell wall thickness of 1.5 mm in multi-material the force experienced by cell size of 3mm is 28% lower than the cell size of 2.5mm. For cell wall thickness of 1.5 mm in multi-material the force experienced by cell size of 2.5mm is maximum. For cell wall thickness of 2 mm in multi-material the force experienced by cell size of 3.5mm is 77.6% lower than the cell size of 2.5mm. For cell wall thickness of 2 mm in multi-material the force experienced by cell size of 3mm is 28.6% lower than the cell size of 2.5mm. For cell wall thickness of 2 mm in multi-material the force experienced by cell size of 2.5mm is maximum.

It is evident that the experimental results are in liaise with the theoretical equation where the thickness of the cell wall increases the force or stress induced increases and if the cell size increases the force or stress induced decreases.

this thesis is dedicated to

“MY FAMILY”

ACKNOWLEDGEMENTS

I am grateful to my supervisor Dr. Yuchun Xu for sharing knowledge and experience with me; for his patience and his endless support. I would also like to express my deepest appreciation to my associate supervisor Dr. Mark Prince for all his support during my time at Aston University and for all his technical advice. I would like to thank Dr. Jeanette Lilly and her team for their help and support. I am thankful to Mr. Dave Upton who helped me during material testing for his perseverance and support. I would like to thank Mr. Rob Thompson sales manager Stratasys Additive Manufacturing company for providing us the fabrication facility and fabricating our components. My gratitude also to Mr. Abdelnasir Omran (a Ph.D. student) and Mr. Mohammed Mito (a Ph.D. student) for their help and support during my research.

TABLE OF CONTENTS **PAGE NO**

LIST OF ABBREVIATIONS

AM	Additive Manufacturing
SL	Stereolithography
FDM	Fused Deposition Modelling
SLS	Selective Laser Sintering
EBM	Electron Beam Melting
MJM	Multi-Jet Modelling
STL	Stereolithography
UV	Ultra-Violet
CAD	Computer Aided Design
MMAM	Multi-Material Additive Manufacturing

FIGURES

TABLES

CHAPTER 1
INTRODUCTION

1.1 BACKGROUND

Much research has been carried out regarding multi-material structure in the area of additive manufacturing including experiments and analysis for the honeycomb structure. Only few researchers have carried out the researches on honeycomb with single material. This paves way for the curiosity to understand the capability of honeycomb structures using multi-material for the application of static and dynamic resistance.

1.2 VARIOUS METHODS OF ADDITIVE MANUFACTURING

1.2.1 STEREOLITHOGRAPHY (SL)

Stereo lithography uses liquid for fabrication by curing or solidifying them using a UV laser to form the final product. This process is similar to any AM process in which the CAD model where segregated into slices in the STL file. The UV laser targets only in the specific location as described in the CAD model for solidification. After the complete fabrication of the part the liquid material which is not solidified is then collected and used for other fabrication [Wong et al., (2012)]. The stereolithographic process is suitable only for the fabrication of single material whereas the present research deals with fabrication using multi-material.

Figure 1 Schematic Representation of Stereolithography Process [Wong et al., (2012)]

1.2.2 FUSED DEPOSITION MODELLING (FDM)

Fused Deposition Modelling is a thin filament based AM process where the filament is melted to a semi solid state by the extruder print head. This process does not involve chemical post processing and the fabrication of multi-material is quite impossible through this technique [Wong et al., (2012)]. So this process cannot be used for the fabrication of variation in digital multi-material, which is the prime factor of the present research.

Figure 2 Schematic Representation of FDM Process [Wong et al., (2012)]

1.2.3 SELECTIVE LASER SINTERING (SLS)

Selective Laser Sintering (SLS) is an AM process, where the product is printed by sintering of powder using CO_2 laser beam. As specified by the CAD model the laser traces the path and fuses the powder at specific coordinates. The powder bed lowers as each layer of material is being fused and another layer of powder is spread over the fabricated layer and then it is again sintered until it reaches the final product [Wong et al., (2012)]. Since this method cannot fabricate combination of metals, ceramics, plastics this fabrication is not suitable for the digital materials which is being used in our research.

Figure 3 Schematic Representation of SLS Process [Liu et al., (2007)]

1.2.4 ELECTRON BEAM MELTING

The Electron Beam Melting machining provides a new technique for the fabrication of metal multi-materials. The initial step involves building the start plate to make sure the fabrication of first material could be press fit to form flat surface, providing the base for secondary material. The fabrication of the metal multi-material involves a 60 keV high energy electron beam which solidifies the metallic powder in layer-by-layer fashion. The metal powders are melted by the electron beam passing through the focussing magnetic lens in a vacuum chamber where the kinetic energy is transferred to powders. Thickness range is about 70-200 µm. Helium gas is used to purge the build chamber and cooling of the solid part after the completion of fabrication with removal of exam powder form the built part [Liu et al., (2016)]**.** This fabrication method involves only metals where our research concentrates on the digital

polymer materials. From the figure 4 the major components include the electron gun (1), magnetic lenses (2), powder contained in the hoppers (3), rake mechanism (4), work piece (5), and build table (6).

Figure 4 Schematic Representation of EBM Process [Terrazas et al., (2014)]

1.2.5 MULTI-JET MODELLING (MJM)

Inkjet technology is used to produce the model in Multi-Jet Additive Manufacturing process. The minimum thickness of fabricating a part through this method is 16µm with high resolution. With this process multiple materials can be built in a single product along with multiple colours also. This process can produce only multiple materials of polymers which is our prime concern. In our case this process is used to produce two materials namely ABS and ELASTOMER in a single part. A UV lamp is attached to the set of nozzles, which is used to deposit the materials, and this UV rays are used to cure the materials, which solidifies the materials, and the support structures are removed in the post processing using water jet [Wong et al., (2012)]. And this research is primarily the continuation of my earlier research work the multi-jet process is considered for the present research.

Figure 5 Schematic Representation of MJM Process [Rajendra Boopathy et al., (2019)]

1.3 MULTI-MATERIAL

AM plays an important role in the high-value manufacturing economy. MMAM provides benefits and opportunities for future challenges and response of business competency in the evolution of global trends and new market drivers. Multi-material AM systems satisfies the need of some applications that single material Additive Manufacturing system fail to carry out from one machine, such as compliant

mechanisms, embedded components, 3D circuits, human tissues, medical compatible implants etc. The novel MMAM technology has the potential to offer these merits: [Vaezi et al., (2013)]

- Freedom of Design: this technology provides a lot of freedom in terms of design and multi-material. It allows us to provide required material properties in the desired areas. Variety of shapes with required functionality could be achieved at specific places in the fabricated product using MMAM. Micro level circuitry, embedded components and small devices can be produced by this system, which results in minimum space requirement of the product [Vaezi et al (2013)]. Since Additive Manufacturing provides a high range of freedom in design, the honeycomb material which is used in the present research work has been given a lot of variations in terms of geometry and multiple materials.
- Increase in Functionality: As we can see from the Additive Manufacturing multi-material process the possibility of fabricating multiple materials which in turn we can decide the functionality of the product. Material and material property integration creates new innovative products with functional gradients, which in fact provides increased functionality [Vaezi et al., (2013)]. Since Additive Manufacturing can produce high range of increased functionality to the product which in turn is incorporated in our research for the honeycomb structure for the static and dynamic behavior applications
- Assembly elimination: fabricating different kinds of multiple materials or even same materials that need assembly is totally eliminated in the Additive Manufacturing process, as we can see all the multiple parts built in one build itself. Hence the process has high productivity and streamlined [Vaezi et al., (2013)]. Our research comprises of multiple materials fabrication in a single product that would involve an assembly operation when it is fabricated conventionally.
- Efficient manufacturing system: Single integrated manufacturing is the main advantage of Additive Manufacturing process which can reduce the time for change over of components between process which is predominant in conventional process [Vaezi et al., (2013)]. Since our research involves fabrication of multi-material the fabrication takes less energy and minimal wastage of materials and the process itself is cost effective.

1.4 HONEYCOMB STRUCTURE

Honeycomb structures are generally inspired from the nature through honeybee combs. The honeycomb structure itself has very high strength to weight ratio which is an advantage of lighter weight and for higher impact resistance. Due to the nature of its structure it provides minimal density of the product. The honeycomb structural behaviour is dependent on the core height, cell size, wall thickness etc., which will be discussed in detail in this research. The applications of honeycomb include panels for roof, beams for bridges, decks for pedestrians and bridge and railway sleepers etc., [Ukken et al., (2017)]. There are types of honeycombs based on their material which include aluminium, nomex, thermoplastic and stainless steel honeycombs

1.5 CRASH WORTHINESS

A rapid leap in the number of injuries to the driver in automobiles made the research to take a diversion towards the crashworthiness. Most studies during the 1980s focussed on engine and steering performance, vibration and driving comfort [Kim et al., (2012)].

Cellular structures like honeycombs, in general, are used for energy absorbing applications to prevent the components from getting damaged [Habib et al., (2018)]. In our research, we use honeycomb structures for the same reason with multiple materials. The application, which we are more concerned about, is the crash resistance like a car bumper, helmet, knee guard, etc., So in automobile industry composite materials are becoming inevitable for crashworthiness and lightweight requirements. These composite structures generally have high specific stiffness, high energy absorption capability and high specific strength [Liu et al., (2016)]. For the cellular structures, the low peak force obtained during the initial plastic deformation evaluates the better performance [Estrada et al., (2016)]. Honeycomb structures contribute high strength-weight ratio, favourable cushioning properties, and lightweight which are more prominent for the aircraft landing gear shock absorbers and high-speed trains [Zhang et al., (2019)].

The selection of cell geometry and cell wall thickness plays a major role in the efficient energy absorption of the component [Habib et al., (2018)]. The imperfection in the geometry of the honeycomb also affects the characteristics of energy absorption [Estrada et al., (2016)].

CHAPTER 2

LITERATURE REVIEW

In this chapter we will be discussing about the various literature surveys of additive manufacturing, crash resistance and cellular structures.

2.1 ADDITIVE MANUFACTURING

Additive manufacturing is used as a tool for fabrication of parts by printing layers of material one over the other with the help of the information available from 3D CAD (Computer Aided Design) model [Dutta et al., (2001)]. In our research we will be using the CAD for the fabrication of honeycomb structures with varying cell size and cell wall thickness. According to the standard ASTM: F2792-12a the need for process planning is totally eliminated in the 3D Printing process in contrast to subtractive manufacturing technologies where the American Society of Testing Materials defined AM as "Process of joining materials layer by layer to make parts using 3D model data. Similarly in 2014 M. Sugavaneswaren et al., suggested a novel methodology for randomly oriented multi-material (ROMM) fabrication using polyjet 3D printing machine. In this they have modelled the multi-material in CAD using CATIA VB SCRIPT where in the reinforcement layer which is considered to be plastic material and the matrix layer which is considered to be elastomer material. They have used the multi-material for the application of stress-strain behavior using UTM (Universal Testing Machine).

In recent years composites are becoming more of interest in the field of 3D printing they are being considered as [S. Kumar and J.P. Kruth et al., (2010)] replacement for metals in many applications especially in mechanical applications, which can also be fabricated using RP (Rapid Prototyping) technique. For the manufacturing of bio-composite scaffolds RP has unique advantages over the conventional manufacturing techniques. The enhancement of the basic process which includes components property improvement or optimization of the final part can be achieved by the multi-material composites specifically polymer based components [Liu et al., (2007)].

The reasons for applying Multi-material strategies are as follows: [Gibson et al., (2010)]

- Inclusion of secondary materials allows improvisation in mechanical properties of polymer parts fabricated through AM.
- Additional material in AM parts itself says additional property which in return provides two or more functions to polymer parts fabricated through AM.
- To separate two regions in a product additional materials used to act as barrier material thereby helping in compliant mechanism fabrication enabling the regions to have a motion relatively

A new highly optimized structure of a component by digital integration of stiffness, composition and toughness creates a new potential to optimization and design in engineering. This is possible through

high aspect ratio fillers which are aligned towards the direction of print. The spatial control of the part orientation is achieved by build path. Fabrication of large range of composite structures which are bio-inspired is suited for this approach with optimized design and mechanical properties [Compton et al., (2014)].

The compact structures created using SLS with gradient flexural properties which showed the parametrically defined rigid pattern has the ability to induce passive bending behavior on structures. The differences in bending stiffness where found to be 20% and 50% for parallel and perpendicular directions with stress redistribution capacity is independent on rigid pattern direction [Munguia et al., (2014)].

The way of manufacturing and supplying products to the customer is revolutionized by the technology of Additive Manufacturing. For redesigning and development of the product the axiomatic design approach is considered. The methods and approaches for conventional manufacturing have certain limitations over Design for Additive Manufacturing. Capability of the process for complex designs by using undiscovered areas of space design and creativity evaluation using 2 axiomatic design theorems is possible through combining axiomatic design with optimization of surface design for decomposition at large level [Salonitis et al., (2016)].

Another study [Yoon et al., (2014)] in biometric structures showed that honeycomb structures are ideal for applications which needs higher strength and toughness. Applications which require high elasticity, tubercular bone structures are ideal structures eg., bone marrow strength characteristics. They come to a conclusion that for the study of biometric structures 3D-printing is an effective way. Following this research a similar research [Lim et al., (2017)] on custom made plastic casts replaced the traditional plaster casts. They used extrusion type 3D-Printing for the fabrication of model involving number of holes for better ventilation and minimum weight for easy handling of the component. Structural safety and stiffness of the cast is evaluated using FE analyses, which then allows us to arrive at higher specific stiffness with improved bending stiffness than the conventionally produced solid structure.

2.2 CRASH RESISTANCE

In 2012 Tejasagar Ambati et al., predicted the behavior of vehicle after collision of frontal crash test with the aid of computer models. It has been observed that at 0.4 seconds from the initiation of crash half the energy is being absorbed by bumper and rails. Similarly Beyene et al., (2014) provided the possibility of obtaining progressive failure in the crash behavior of frontal and rear bumper through composite materials rather than steel. They achieved this by having various sections along the length of the structure and integrating the same. Safety in crash and demands in lightweight of bumper system has been proposed in an effective way using composite structures. The optimization procedures of integral bumper system provides crashworthiness and strength requirements with reduced weight [Liu et al., (2016)]. There are specifically some optimization methods for design like multiple regression

methods in Design of Experiments are quite useful in optimal design development for maximum energy absorption per unit weight and their evaluation for the side members. They have concluded that fatigue crack growth rate is higher in the transverse direction of the grain orientation, which signifies shorter fatigue life. A sequential and ideal deformation was found to occur in the axial compressive deformation. Reduction in human number and cost effectiveness was expected that would replace the high cost energy absorption system to the efficient and improved internal crash energy system [Kim et al., (2012)].

2.3 CELLULAR STRUCTURES

In 2005 Zhao et al., conducted the experimental study on impact resistance of aluminium honeycomb structures. They have included various cell size and thickness, which exhibited 15% strength enhancement over dynamic loading that concluded that the micro-inertia effect in the successive folding of honeycomb has a major role in strength enhancement.

The rate of stress between grades of aluminium honeycombs increases due to strain hardening. The effect of inertia has a predominant role in cellular materials under quasi-static and dynamic loading where the crushing pressure is enhanced through the folding of honeycomb [Hou et al., (2012)]. The aluminium honeycomb crushing pressure is affected by the loading rate. They have also concluded that the large enhancement of crushing strength is not due to the increase in aluminium foil flow stress between compressive and impact loading [Zhao et al., (1998)]. In 1998 W.E. Becker et al used thin walled aluminium and steel honeycombs to study the capacity to absorb energy by these two different materials including strain rate effect. A testing method has been developed for a high compressive deformation of the honeycomb specimens in a state approximating uniaxial strain. A 32% density ratio of solid aluminium in aluminium honeycombs and 37% density ratio of solid steel in steel honeycombs are used for this testing method. It seems that both the aluminium and steel honeycombs tend to have a strain rate effect from their results. Applications involving significant reduction in out-of-plane motion with increased energy absorption and decreased buckling this technique could be considered. The stress distribution of the aluminium honeycombs where found to increase with the inclusion of ‘through the thickness’ insert types in both theoretical and Finite Element models. Therefore, the relative placement or position of the inserts in the honeycomb provide a drastic effect over the stress distribution [Slimane et al., (2008)]. During the experimental and analytical investigation of mechanical behavior of aluminium honeycombs epoxy along with adding MWCNT(Multi-Wall Carbon Nano Tube) gave increased power values with decrease in cell width and height with 85% reliability of results between experimentation and analysis [Akkus et al., (2017)]. Since the aluminium honeycombs are generally energy absorbing structures which can be used for the application of energy absorption in satellite design. They are mainly used for the prevention of interaction between the electronic parts within the satellite which leads to their damage. In this case the numerical and experimental results with respect to energy absorption were found to contradict with less than 6% [Salem et al., (2017)].

A methodology was proposed by F.N.Habib et al (2018) for balancing the energy absorption using cell shape and its arrangement in the honeycomb selection for in-plane energy absorption application. It was found that from a range of different honeycomb cell structure the hexagonal honeycomb seems to have the best energy absorbing behavior and coincides 80% with the ideal energy absorber behavior. The buckling deformation and undulating stress-strain effect continue to dominate in the plateau region as the buckling to bending member ratio increases. Although they found that the hexagonal honeycomb was the best they also concluded that the triangular and regular quadratic honeycomb have advantages over the energy absorption applications due to their maximum initial peak stress than plateau stress. The dynamic response of honeycombs with different cell geometry is crucial for the safe use of honeycombs involving various applications in engineering.

A study on [Zhang et al., (2016)] investigation of hastealloy-X honeycomb and GH4169 double stepped labyrinth behavior under rubbing action at maximum speed with variation in blade tip speed is performed to increase the efficiency of turbo-engines. Due to a higher speed, the damage including thermal ablation and oxidation were bound to occur on the blade tip. In our research, the honeycomb structure is used similar to the above research that involves compression deformation for the crash resistance application.

A mathematical model has been developed by Hui et al (2017) namely, composite structure optimization model and simply supported beam model for a variety of multi-materials. The comparison for the above models are made for both single and multi-material, where the stiffness optimization coincides with the mechanical properties of the materials. Similar to the above study a homogenization approach [Ziegler et al., (2017)] for mechanical performance simulation without any detailing in cellular components modelling serves the purpose for parameterization of the material model mechanical tests including shearing and bending have been performed. The strength and stiffness of the material has been overestimated by the homogenized model in shearing and where verified to work on curved structures also. In this case the cell structures are adapted according to the pre-determined load for the mechanical behavior improvisation of the whole component. The hexahedron structures have been replaced by the still inserts. Using the 3D printing technology they have also fabricated a life size cantilever chair with inclusion of cellular structures.

Several authors proposed variety of strategies using cellular structures for the adaptation to energy absorbing applications one among which Fábio Ribeiro Soares da Cunha et al (2014) proposed a strategy for energy based robustness measures which includes ultimate and collapse load, energy based robustness index, energy reserve and energy until limit. These requirements are satisfied by their proposed strategy. The final optimal best design using the proposed strategy selected is the lightweight design with strength and robustness, which collapses under ultimate load. Similar to the above research Guo-Hua Song et al (2017) proposed a theory that there is an enormous potential for the irregular cellular structure, fabricated using Additive Manufacturing for the application of lower mass design. The design

instructions are provided by this theory to fabricate irregular cellular structures. The fabricated cellular structures have been optimized using variable density optimization theory. The experimentation and simulation results have similar behavior indicating the maximum deformation for SIMP(Solid Isotropic Microstructures with Penalization) is ahead of the modified version under same load. The study concluded the following (1)For the automatic generation of the main outline of cellular structure, an irregular cellular structure realization method is proposed using tangent circles principles. (2) The irregular cellular structure is optimized due to the employment of modified SIMP approach using relative density information. (3) The results through experimentation show that the SIMP approach deformation is 5.4910-5mm ahead of the modified SIMP approach for irregular cellular structure.

In 2017 Yiru ren et al proposed the best ratio of stepped circular and square tubes strut system for the application of strut crashworthiness in aircraft. For improved impact resistance characteristics under axial load, the stepped thin-walled characteristics under axial load the stepped thin-walled tubes where found to have significant performance. Since the origin of the failure appears to be in the stepped thin-walled tubes joint, the radius, thickness and step width determine the load force efficiency. A 2:1 ratio is the best length ratio for stepped circular tubes and a 1:1 ratio for the square tubes between the upper and lower sections. Similarly in 2015 Quirino Estrada et al presented the implementation of geometric imperfections for the energy absorbing characteristics of steel structures through a numerical explanation. In this case, structural discontinuities play a major role in energy absorption performance. These discontinuities with the curved form provided a significant performance of 12.54% energy absorption and a reduction in peak load of 22.13% by the diamond-shaped discontinuities inclusion. This proves that the aspect ratio and shape discontinuity influences the energy absorbing capacity than the cross-sectional area. Another study [Darvizeh et al., (2014)] on energy absorption and mechanism of deformation provided the energy absorbing characteristics of grooved circular tubes under quasi-static loading condition. The thin-walled tubes offer the stabilization of the tube by dividing the thick-walled tubes. The improvisation of analytical formulation values coincides with the experimental values through the inclusion of the effect of strain hardening in flow stress and the effect of variation on the circumferential strain. To determine groove length, wall thickness and number of groove for crashworthiness improvement this work should be useful.

In 2015 K. W. Hou et al used sinusoid corrugation to create a new double-sine-wave which is embedded in the axial and transverse directions with the adjacent ones having phase difference. A theoretical model is adopted for the mean crushing load prediction of the rigid plastic material and numerical simulation under axial crushing of staggered double-sine-wave-tube using hyper mesh and LS-dyna. From the results it was observed that wall thickness, corrugation numbers in axial & transverse direction and depth of corrugation are the main reasons for influencing the staggered double-sine-wave energy absorption. This shows low load uniformity and initial peak load is in divergence with straight tube. This could be used for the applications involving equipment or people protection against energy.

From the literature survey it is observed that very few work has been carried out on crash analysis in particular on additive manufactured honeycomb structures and also optimization with respect to multi-material in honeycomb structures.

CHAPTER 3

THESIS SCOPE

3.1 AIM: To investigate the effect of cell wall thickness and cell size of additive manufactured honeycomb structures using multi-materials with the help of a theoretical model on energy absorbing characteristics.

3.2 OBJECTIVE

- **i.** To use a theoretical model for static and dynamic analysis.
- **ii.** To model the honeycomb structure with various cell wall thickness and cell size using CATIA software.
- **iii.** To fabricate the single and multi-material honeycomb structure using polyjet.
- **iv.** Conducting static testing of the fabricated models.
- **v.** Conducting static and dynamic analysis using ABAQUS software.
- **vi.** Validation of experimental results with analytical results.

3.3 SUMMARY OF CHAPTERS

This thesis consists of six main chapters including Introduction chapter. Below are the brief description of the following five chapters:

Chapter 2: In this chapter, literature review is covered.

Chapter 3: In this chapter, Aim, Objective and Methodology is covered.

Chapter 4: In this chapter, Design and analysis is covered.

Chapter 5: In this chapter, Experimentation is covered.

Chapter 6: In this chapter, Results and discussion is covered.

Chapter 7: In this chapter, Conclusion is discussed.

3.4 METHODOLOGY

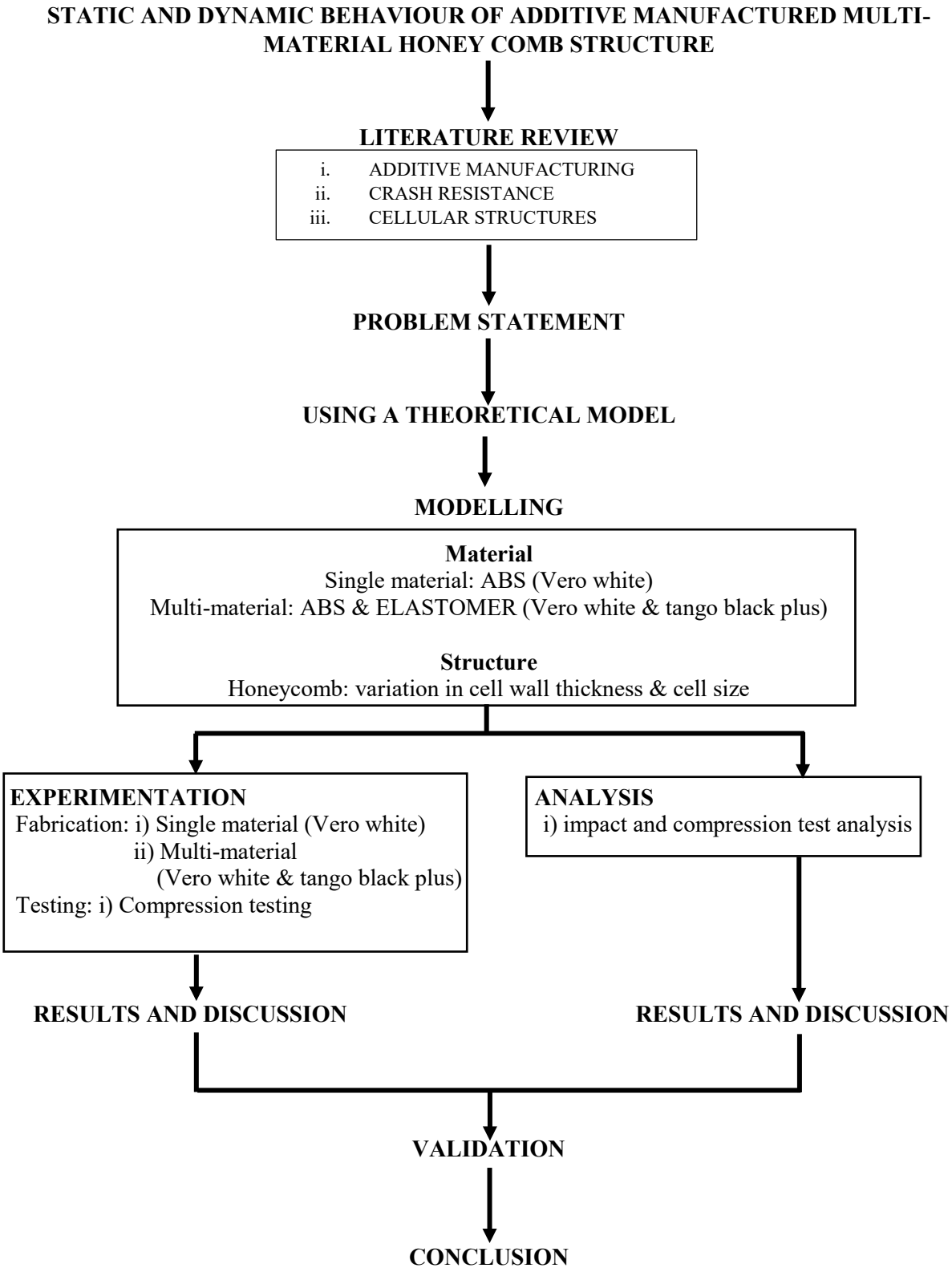

The methodology involves peer review of literature in the research area of additive manufacturing involving fabrication of honeycomb structures, multi-material followed by crash resistance application where it is involved more and the basic mechanism behind the energy absorption of crash resistance. The main criteria behind energy absorption are found. Then some literature studies are made regarding cellular structures of how it affects the static and dynamic loading. From all the inference collected from the literature the problem statement is defined. From the problem statement we included a theoretical model for modelling of both single and multi-material honeycomb structure. The theoretical model involves the buckling member as the main criteria. After this the single and multi-material honeycomb structures are modelled with variation in cell wall thickness and cell size using CAD modelling software CATIA V5R20 in accordance with the buckling member criteria. Using this modelled honeycomb structures impact and compression analysis are carried out using the ABAQUS software. On the other hand single and multi-material honeycombs are fabricated which then undergoes compression testing only. The results of impact and compression analysis was discussed and the results of experimental compression testing was also discussed. Finally the results of analytical and experimental compression analysis are validated. Conclusions are given based on the analytical results of both impact and compression analysis along with experimental results of compression testing on how it correlates with the theoretical model.

CHAPTER 4

DESIGN AND ANALYSIS

4.1 FACTORS TO BE CONSIDERED FOR THE MODEL

- Young's modulus of each material E.
- Poisson's ratio (lateral strain/axial strain).
- Cell wall thickness and cell wall size.
- Number of stacking of material layers and shape of cellular material.

4.2 THEORETICAL MODEL

For the purpose of modelling the multi-material honeycomb structure, a theoretical background [Vincent et al., (2013)] of buckling of cell walls is considered. Vincent et al have considered this theoretical model for normal impact of honeycomb cell walls. In our research the elastomer is considered as buckling member in multi-material and ABS in single material.

$$\sigma_{cs} = K \cdot \frac{\pi^2 E_s}{12 \cdot (1 - \nu^2)} \cdot \left[\frac{T}{L}\right]^2$$

For a constant cell wall thickness of honeycomb, the expression can be written as:

$$\sigma_{ch} = 1.044 \cdot K \cdot E_s \cdot \left[\frac{T}{L}\right]^3$$

And they have constraint regarding the buckling member where height 'b' should be large compared with 'a' i.e. b>3L with constant 'K' as end constraint factor [Zhang et al., (1992)]. Where 'T' is cell wall thickness, 'K' is buckling factor and 'L' is cell wall size, 'Es' is Young's modulus of the material and 'ν' is Poisson's ratio of material.

4.3 COMPUTER AIDED MODELLING

AM process takes 3D solid CAD model as input for machine instruction to move the controller and deposit the material where it is required. But most of the CAD modeling software represents the part only with homogeneous material, which is difficult to represent multiple materials of composite materials. Furthermore, majority of AM process take CAD model in STL format as standard input. Since STL is a surface approximation only, there is no knowledge of the material representation. Hence for the purpose of representing multiple materials for region to region, Boolean operation coupled with assembly operation were used to create CAD model with multiple material (one part for matrix and another part for reinforcement) as shown in figure 6.

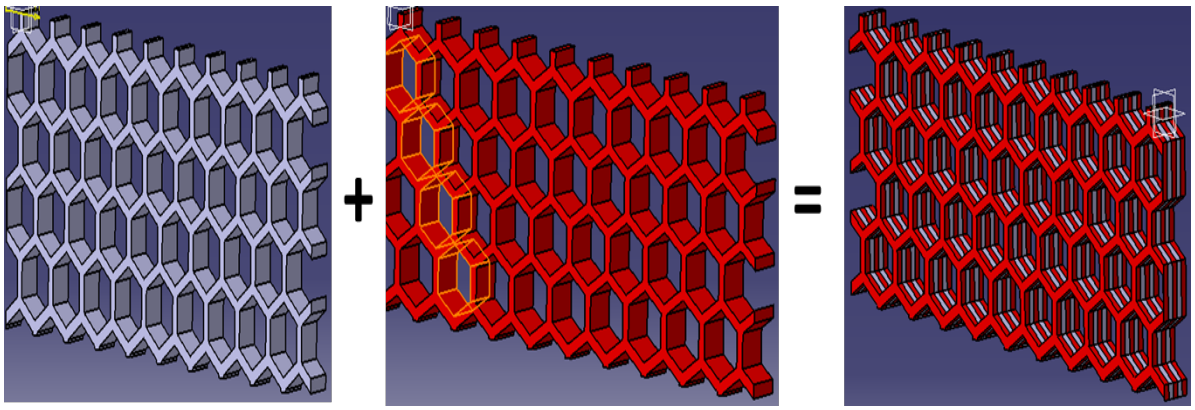

Matrix reinforcement matrix + reinforcement

Figure 6. Flow chart for modelling multi material for AM process

4.4 MATERIALS FOR HONEYCOMB STRUCTURE

As mentioned earlier, the materials used in PolyJet 3DP technique are photopolymers, meaning they are solidified under the action of UV light. PolyJet 3DP can process wide range of polymer materials with different properties to provide greater strength, stiffness, heat deflection, etc. This wide range of polymer includes high strength ABS, flexible polypropylene, and rubber like elastomers. Exact details of these materials are undisclosed but they were named under the trade mark name (e.g. Tango plus, Vero white, Durus white, etc.,) provided by the machine supplier. Table I Summarize properties of polyjet 3DP polymer materials considered for analysis of crash test for multi material structure.

Table 1 Properties of polymer material considered for non-linear analysis of multi material honeycomb structured honeycomb structure

Sl. No.	Properties	Materials	
		Vero White (Reinforcement)	Tango plus (Matrix)
1	Tensile strength (MPa)	50	1.8-2.4
2	Elongation at break (%)	20	130-150
3	Young's modulus (MPa)	(2000-3000)	(0.1 - 0.3)

4.5 STATIC ANALYSIS USING ABAQUS SOFTWARE

For the analytical method ABAQUS software is used to perform static behaviour and the following are the steps conducted to perform them.

i. Part
In this process the modelled part is imported into the abaqus software using .stp format.

ii. Property
In this section the property of the material is assigned like density, young's modulus, Poisson ratio and hyper elastic property. For multi-material the stiff material vero white is assigned with density, young's modulus and Poisson ratio and for the rubber like material tango black plus the hyper elastic property alone is given specifically for static analysis. And then separate section is created for each part single and multi-material parts with homogeneous solid section and these sections are assigned with specific material property to the specific parts.

iii. Assembly
The parts with assigned property are then assembled in this section.

iv. Step
A time step is created for the simulation of static analysis in which the step procedure is created as static, general and also includes time period and incrementation of time. In this section the time period and incrementation of time is adjusted in such a way that the load that is given as input is converted to static load.

v. Interaction
In this section the interaction property is given for in between materials, so largely it cannot be used for single materials. For compression testing the self-contact and tie contact interaction is given in between two different materials.

vi. Load
In this section the model is constrained in all three directions on one surface of the honeycomb and the other axial side surface of the honeycomb is constrained with displacement and rotation i.e, it is constrained in x and y direction and the displacement value of the axial surface is given in the z direction as shown in figure.

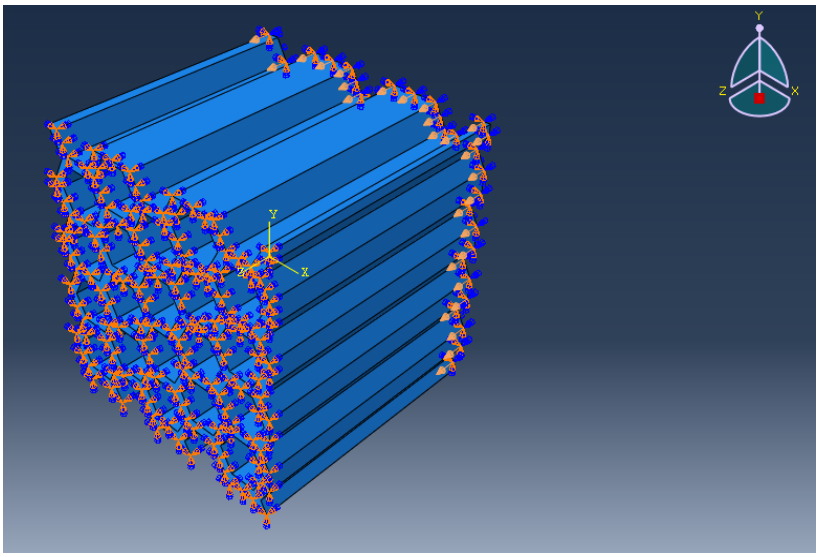

Figure 7. Load constraint in honeycomb structure during static analysis

vii. Mesh

In the mesh section the parts are then assigned with mesh size required and then they are meshed to obtain the required number of elements.

viii. Simulation

After the model is meshed then the model is submitted for analysis and simulation. After the completion of simulation the Force vs Displacement graph is plotted by selecting one of the unique nodes from the mesh.

4.6 DYNAMIC ANALYSIS USING ABAQUS SOFTWARE

For the analytical method ABAQUS software is used to perform static behaviour and the following are the steps conducted to perform them.

i. Part

In this process the modelled part is imported into the abaqus software using .stp format.

ii. Property

In this section the property of the material is assigned like density, young's modulus and Poisson ratio. For multi-material the stiff material vero white is assigned with density, young's modulus and Poisson ratio and the same follows for the rubber like material tango black plus in dynamic analysis. And then separate section is created for each part single and multi-material parts with homogeneous solid section and these sections are assigned with specific material property to the specific parts.

iii. Assembly

The parts with assigned property are then assembled in this section.

iv. Step

A time step is created for the simulation of static analysis in which the step procedure is created as static, general and also includes time period and incrementation of time.

v. Interaction

In this section the interaction property is given for in between materials, so largely it cannot be used for single materials. For compression testing the self contact and tie contact interaction is given in between two different materials.

vi. Load

In this section the model is constrained in all three directions on one surface of the honeycomb and the other axial side surface of the honeycomb is constrained with displacement and rotation i.e, it is constrained in x and y direction and the velocity is given in the z direction.

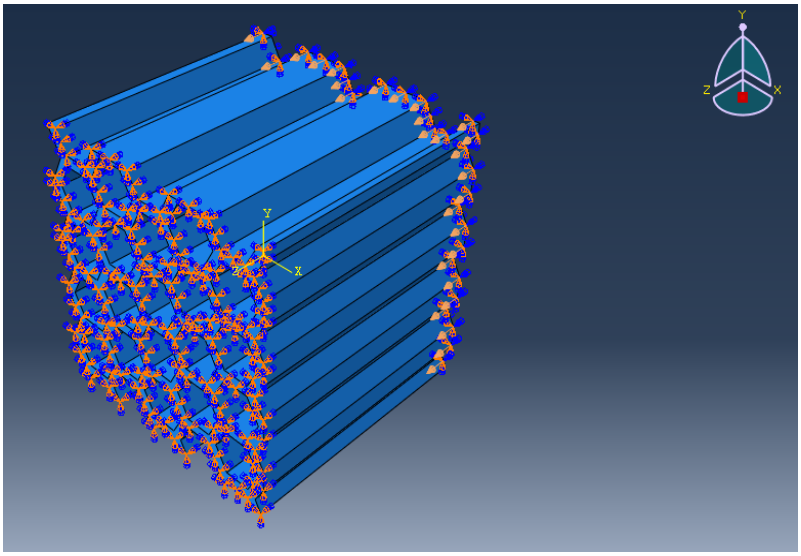

Figure 8 Load constraint in honeycomb structure during impact analysis

vii. Mesh

In the mesh section the parts are then assigned with mesh size required and then they are meshed to obtain the required number of elements.

ix. Simulation

After the model is meshed then the model is submitted for analysis and simulation. After the completion of simulation the Force vs Time graph is plotted by selecting one of the unique nodes from the mesh.

CHAPTER 5

EXPERIMENTATION

5.1 FABRICATION OF HONEYCOMB STRUCTURE

The selected PolyJet 3DP technique for fabrication of polymer based material works under the mechanism where droplets of photo curable polymer resin were deposited through nozzle head as shown in Figure 5, whereas one set of nozzle will deliver one type of polymer material and another set of nozzle will deliver another type of polymer material. So with this construction, two polymer materials were deposited either within a layer or layer by layer with a thickness of about 30 µm. UV light is employed to cure these photo curable polymer resin. In addition, polymer parts can be fabricated by depositing a polymer resin with differing ratio which results in various mechanical properties.

After the fabrication is complete the specimens are overlapped with support structure fullcure which is then allowed to post process. The post processing procedure involves high pressure water gun treatment to remove all of the support structure and then the specimen is illuminated with white light for 12 hours in a closed chamber. Figure 9 show the various models of honeycomb structures for fabrication.

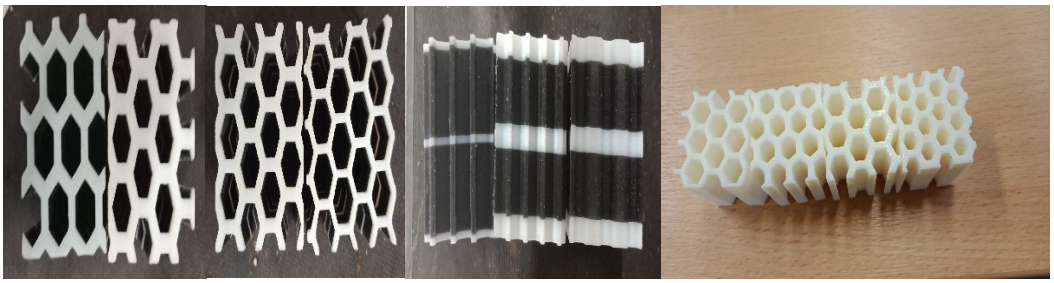

Figure 9 Fabricated Single Material and Multi-material honeycomb structures

- Vero white
- Tango Black Plus

Single material

i) cell wall size (l) - 3.5, 3, 2.5 mm
cell wall thickness (t) - 1, 1.5, 2 mm

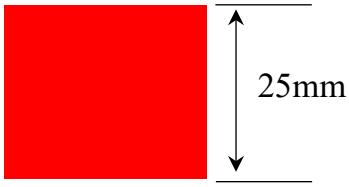

5Layered sandwich multi-material honeycomb Structure

cell wall thickness (t) - 1, 1.5, 2 mm
cell wall size (l) – 3.5mm, depth (b) – 11mm

cell wall size (l) – 3mm , depth (b) – 9.5mm

cell wall size (l) – 2.5mm, depth (b) – 8mm

(a)

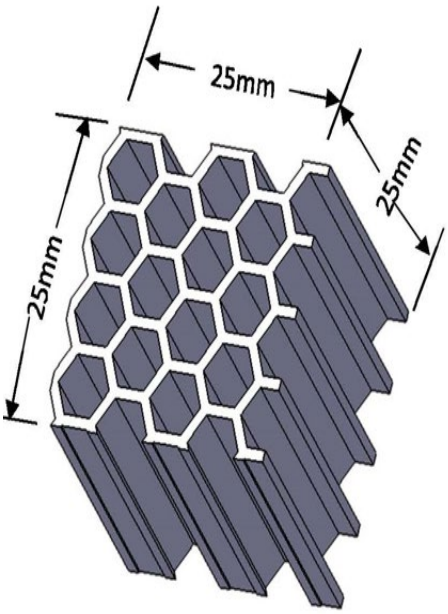

(b)

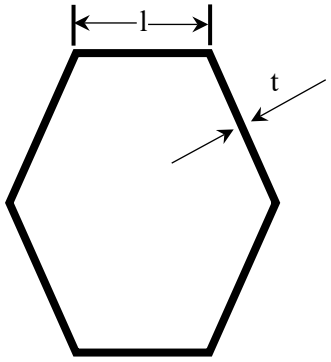

(c)

Figure 10 Models of honeycomb structure for fabrication (a) variation in material thickness (b) 3D model dimensions (c) dimension of single honeycomb

5.2 STATIC TESTING OF HONEYCOMB STRUCTURE

The experimental analysis of compression testing was carried out on single and multi-material honeycombs using the standard instron compression testing machine as shown in figure 11. The dimensions of the specimen are given in the computer input data. The strain rate was set as 4mm/s. the specimen is placed in the flat base was fixed and the other end of the movable flat base was brought closer to the specimen axial direction and then the loading is started and continued until the given amount of displacement which is 23mm.

Figure 11 Instron Compression Testing Machine

CHAPTER 6
RESULTS AND DISCUSSION

In this chapter we will be discussing about the results of the dynamic and static analysis along with static experimentation and validation of static analysis with experimentation

6.1 SINGLE MATERIAL DYNAMIC FINITE ELEMENT ANALYSIS

The dynamic FEA analysis is carried out for single material for various cell wall thickness and cell size in this section.

6.1.1 Cell wall thickness 1 and cell size 2.5

From the figure 12 we can observe that the honeycomb specimen has returned all the kinetic force to the impactor because the single material vero-white has very high composition of stiffness having cell wall thickness 1mm and cell size 2.5mm. This has resulted in maximum rebound of the impactor experiencing a maximum force of 2kN within a short span of time period of .005mS.

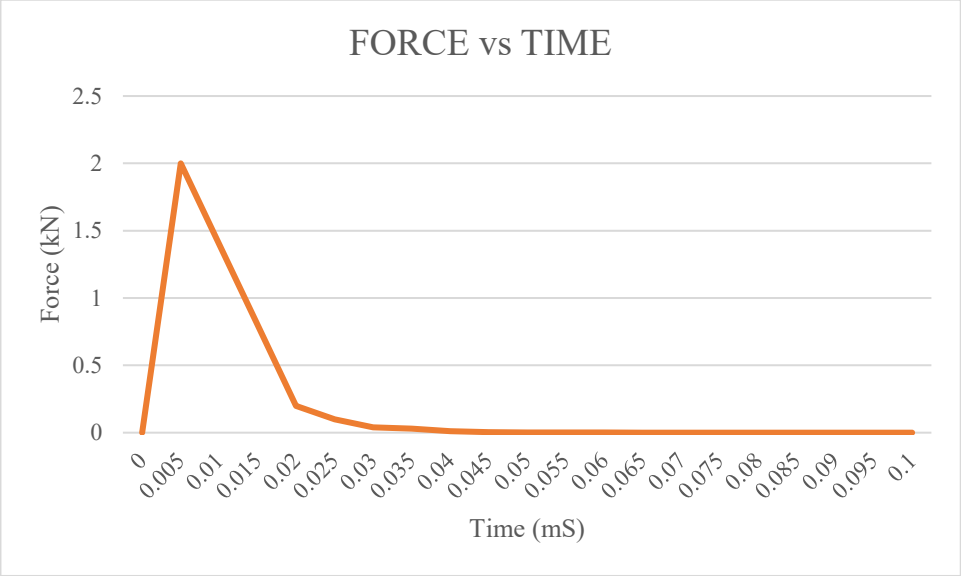

Figure 12. Dynamic FEA Force vs Time curve of single material t-1mm and l-2.5mm

6.1.2 Cell wall thickness 1 and cell size 3

From the figure 13 we can observe that the honeycomb specimen has returned all the kinetic force to the impactor because the single material vero-white has very high composition of stiffness having cell wall thickness 1mm and cell size 3mm. This has resulted in maximum rebound of the impactor experiencing a maximum force of 1.57kN within a short span of time period of .015mS.

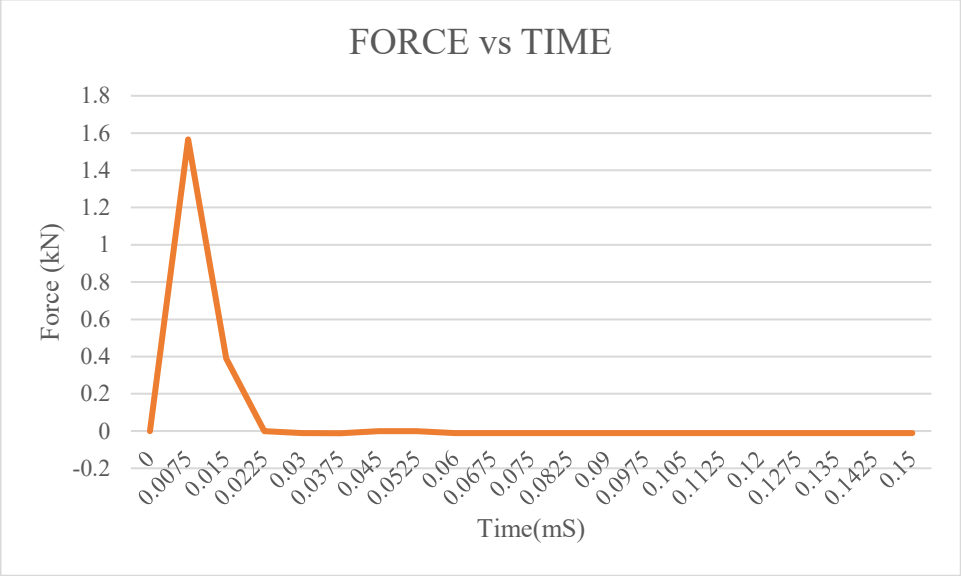

Figure 13. Dynamic FEA Force vs Time curve of single material t-1mm and 3mm

6.1.3 Cell wall thickness 1 and cell size 3.5

From the figure 14 we can observe that the honeycomb specimen has returned all the kinetic force to the impactor because the single material vero-white has very high composition of stiffness having cell wall thickness 1mm and cell size 3.5mm. This has resulted in maximum rebound of the impactor experiencing a maximum force of 1.5kN within a short span of time period of .01mS.

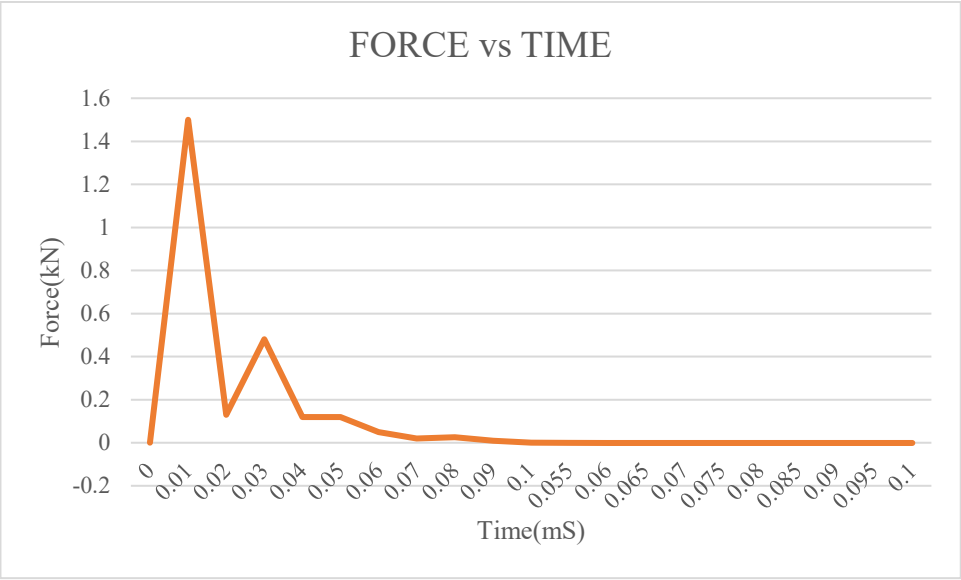

Figure 14. Dynamic FEA Force vs Time curve of single material t-1mm and l-3.5mm

6.1.4 Cell wall thickness 1.5 and cell size 2.5

From the figure 15 we can observe that the honeycomb specimen has returned all the kinetic force to the impactor because the single material vero white has very high composition of stiffness having cell wall thickness 1.5mm and cell size 2.5mm. This has resulted in maximum rebound of the impactor experiencing a maximum force of 4.25kN within a short span of time period of .0075mS.

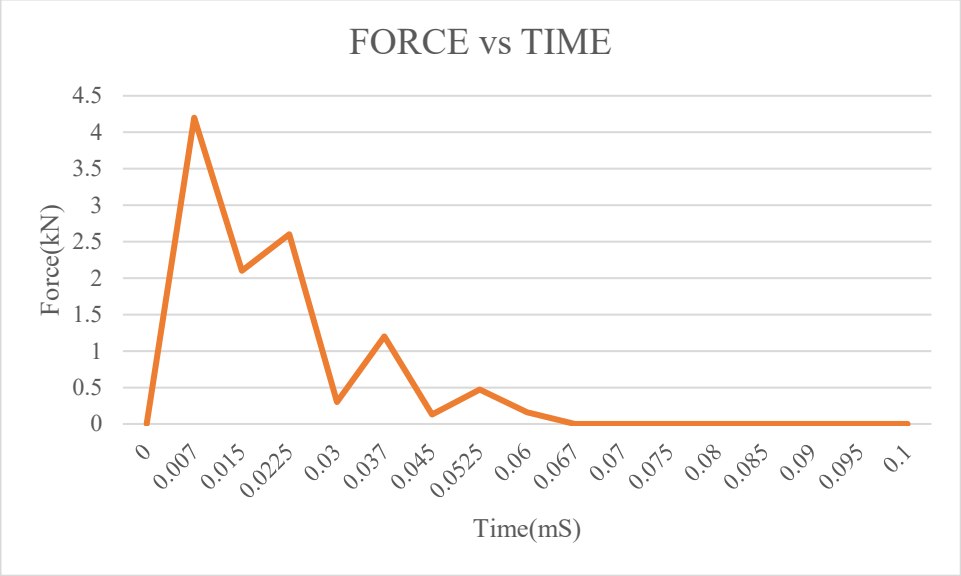

Figure 15. Dynamic FEA Force vs Time curve of single material t-1.5mm and l-2.5mm

6.1.5 Cell wall thickness 1.5 and cell size 3

From the figure 16 we can observe that the honeycomb specimen has returned all the kinetic force to the impactor because the single material vero-white has very high composition of stiffness having cell wall thickness 1.5mm and cell size 3mm. This has resulted in maximum rebound of the impactor experiencing a maximum force of 3.75kN within a short span of time period of .008mS.

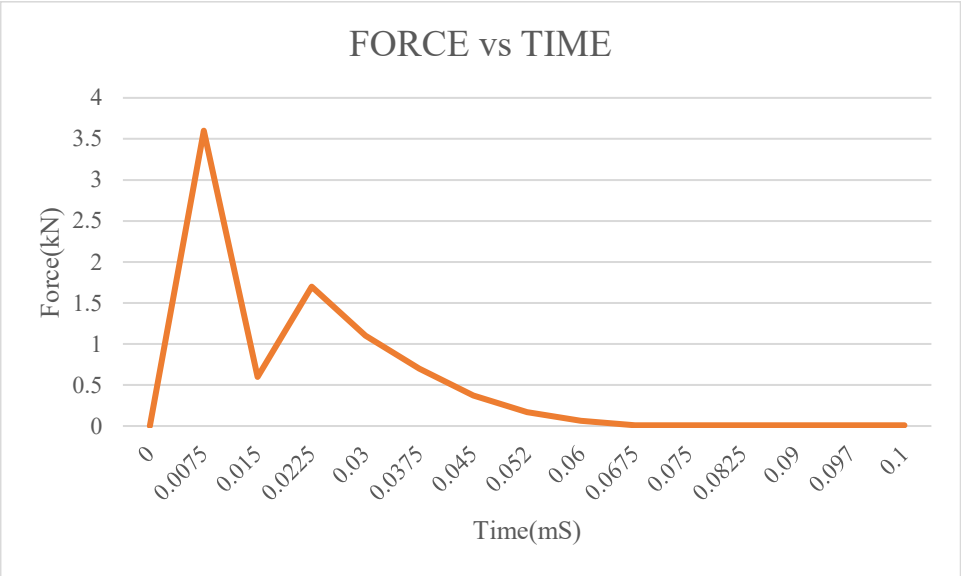

Figure 16. Dynamic FEA Force vs Time curve of single material t-1.5mm and l-3mm

6.1.6 Cell wall thickness 1.5 and cell size 3.5

From the figure 17 we can observe that the honeycomb specimen has returned all the kinetic force to the impactor because the single material vero-white has very high composition of stiffness having cell wall thickness 1.5mm and cell size 3.5mm. This has resulted in maximum rebound of the impactor experiencing a maximum force of 3.5kN within a short span of time period of .015mS.

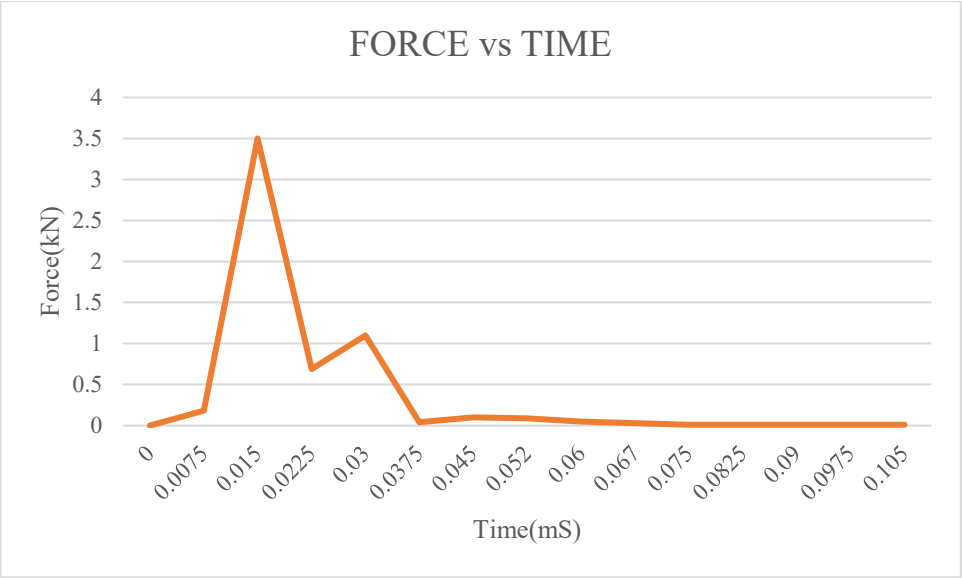

Figure 17. Dynamic FEA Force vs Time curve of single material t-1.5mm and l-3.5mm

6.1.7 Cell wall thickness 2 and cell size 2.5

From the figure 18 we can observe that the honeycomb specimen has returned all the kinetic force to the impactor because the single material vero-white has very high composition of stiffness having cell wall thickness 2mm and cell size 2.5mm. This has resulted in maximum rebound of the impactor experiencing a maximum force of 3.5kN within a short span of time period of .01mS.

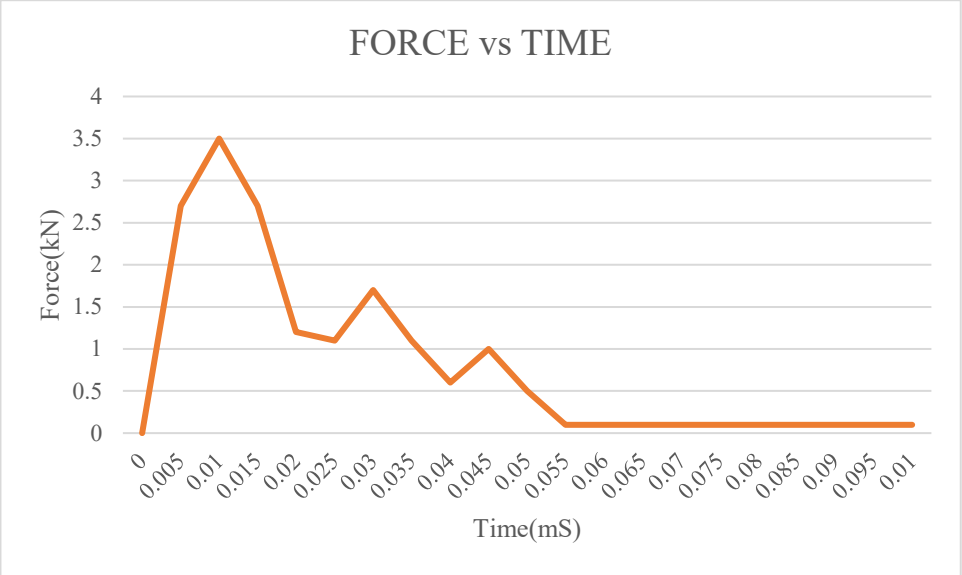

Figure 18. Dynamic FEA Force vs Time curve of single material t-2mm and l-2.5mm

6.1.8 Cell wall thickness 2 and cell size 3

From the figure 19 we can observe that the honeycomb specimen has returned all the kinetic force to the impactor because the single material vero-white has very high composition of stiffness

having cell wall thickness 2mm and cell size 3mm. This has resulted in maximum rebound of the impactor experiencing a maximum force of 2.5kN within a short span of time period of .005mS.

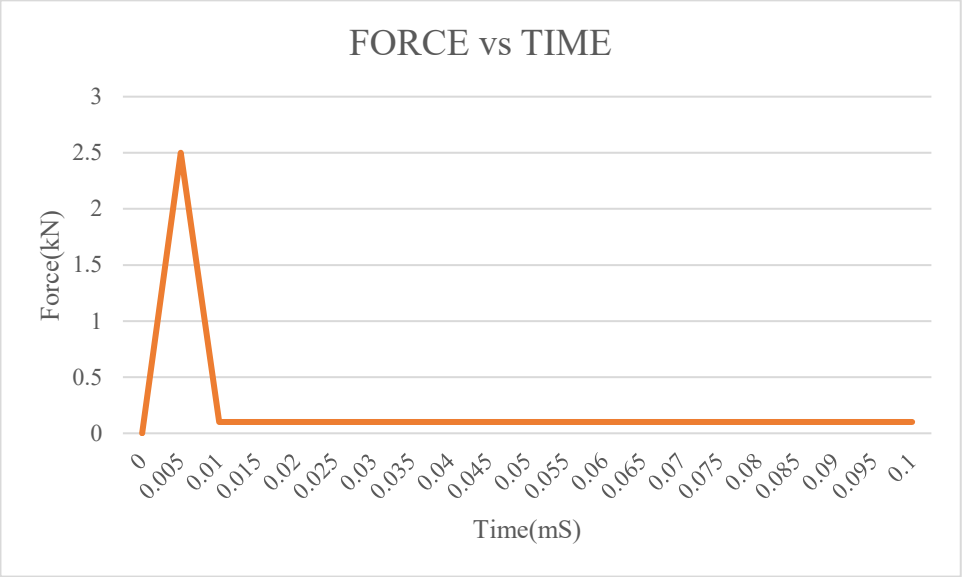

Figure 19. Dynamic FEA Force vs Time curve of single material t-2mm and l-3mm

6.1.9 Cell wall thickness 2 and cell size 3.5

From the figure 20 we can observe that the honeycomb specimen has returned all the kinetic force to the impactor because the single material vero-white has very high composition of stiffness having cell wall thickness 2mm and cell size 3.5mm. This has resulted in maximum rebound of the impactor experiencing a maximum force of .09kN within a short span of time period of .008mS.

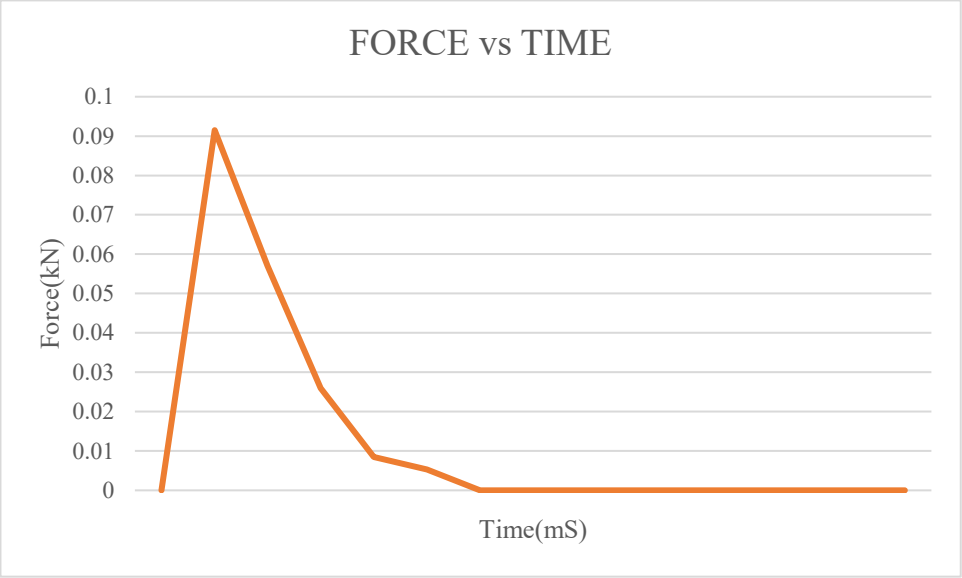

Figure 20. Dynamic FEA Force vs Time curve of single material t-2mm and l-3.5mm

6.2 Multi-material DYNAMIC FINITE ELEMENT ANALYSIS

The dynamic FEA analysis is carried out for single material for various cell wall thickness and cell size in this section.

6.2.1 Cell wall thickness 1 and cell size 2.5

From the figure 21 we can observe that the material experience a progressive failure. At .016kN in .007ms it is observed that there is a kink in the horizontal direction of the curve which shows that the elastomer is absorbing the velocity of the impactor at constant force. Then again the force experienced by the impactor increases to 0.11kN in 0.015ms, the force from the elastomer is transferred to stiff material without much deflection. Then again the force experienced by the impactor increases to 0.12kN and then the force gets decreased indicating the material has failed ultimately where in it is unable to resist the velocity of the impactor.

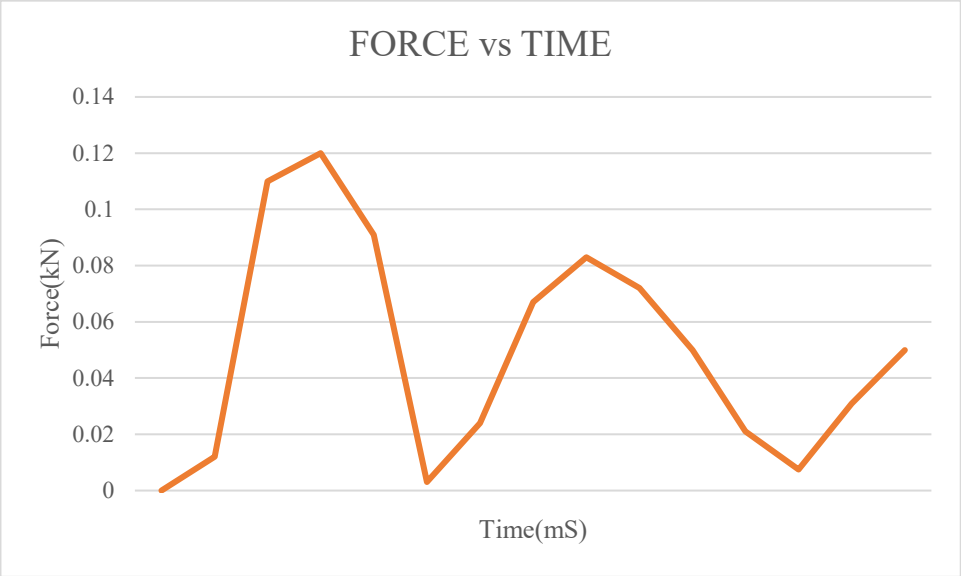

Figure 21. Dynamic FEA Force vs Time curve of Multi-material t-1mm and l-2.5mm

6.2.2 Cell wall thickness 1 and cell size 3

From the figure 22 we can observe that the material experience a progressive failure. At 0.08kN in 0.008mS it is observed that there is a kink in the horizontal direction of the curve which shows that the elastomer is absorbing the velocity of the impactor at constant force. Then again the force experienced by the impactor increases to 0.1kN in 0.023mS, the force from the elastomer is transferred to stiff material without much deflection. Then again the force experienced by the impactor increases to 0.11kN and then the force gets decreased indicating the material has failed ultimately where in it is unable to resist the velocity of the impactor.

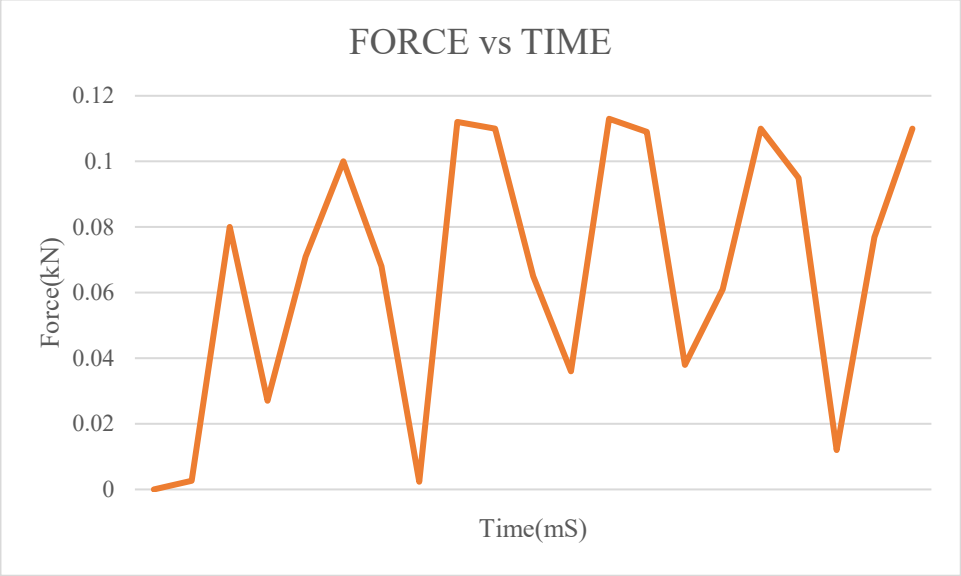

Figure 22. Dynamic FEA Force vs Time curve of Multi-material t-1mm and 3mm

6.2.3 Cell wall thickness 1 and cell size 3.5

From the figure 23 we can observe that the material experience a progressive failure. At 0.04kN in 0.01ms it is observed that there is a kink in the horizontal direction of the curve which shows that the elastomer is absorbing the velocity of the impactor at constant force. Then again the force experienced by the impactor increases to 0.45kN in 0.02ms, the force from the elastomer is transferred to stiff material without much deflection. Then again the force experienced by the impactor increases to 0.5kN and then the force gets decreased indicating the material has failed ultimately where in it is unable to resist the velocity of the impactor.

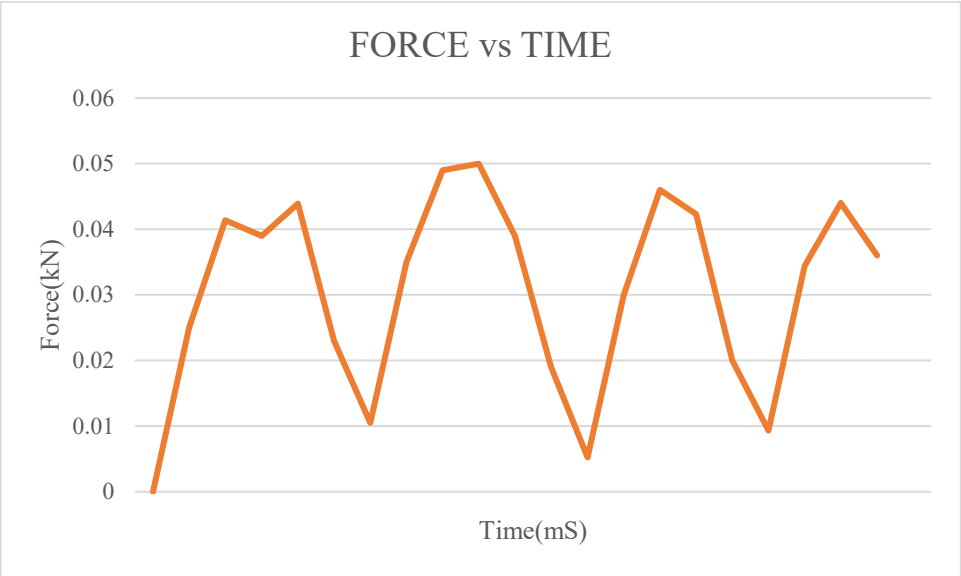

Figure 23. Dynamic FEA Force vs Time curve of Multi-material t-1mm and l-3.5mm

6.2.4 Cell wall thickness 1.5 and cell size 2.5

From the figure 24 we can observe that the material experience a progressive failure. At .05kN in .005ms it is observed that there is a kink in the horizontal direction of the curve which shows that the

elastomer is absorbing the velocity of the impactor at constant force. Then again the force experienced by the impactor increases to .25kN in 0.01ms, the force from the elastomer is transferred to stiff material without much deflection and then the force gets decreased indicating the material has failed ultimately where in it is unable to resist the velocity of the impactor.

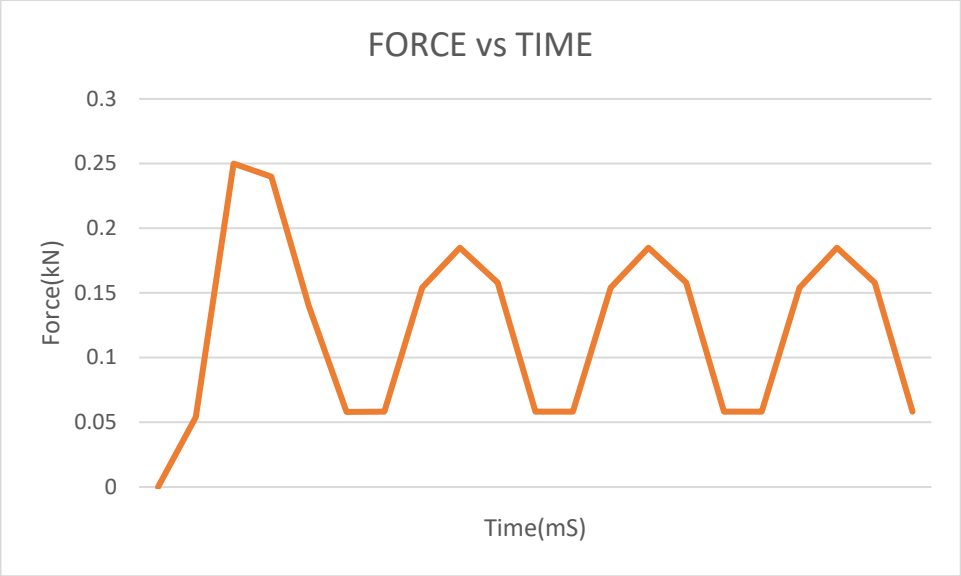

Figure 24. Dynamic FEA Force vs Time curve of Multi-material t-1.5mm and l-2.5mm

6.2.4 Cell wall thickness 1.5 and cell size 3

From the figure 25 we can observe that the material experience a progressive failure. At 0.08kN in 0.01ms it is observed that there is a kink in the horizontal direction of the curve which shows that the elastomer is absorbing the velocity of the impactor at constant force. Then again the force experienced by the impactor increases to 0.12kN in 0.04ms, the force from the elastomer is transferred to stiff material without much deflection. Then again the force experienced by the impactor increases to 0.15kN.

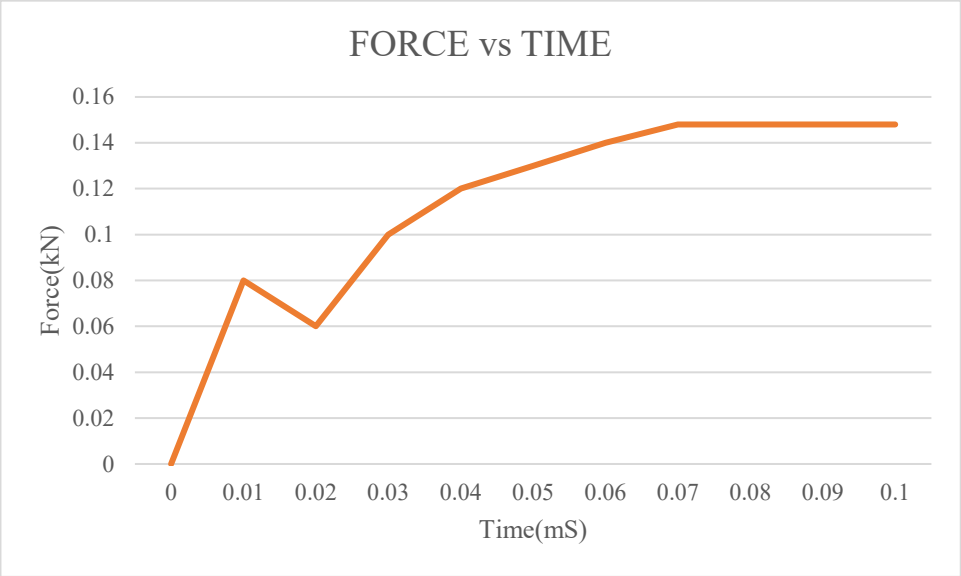

Figure 25. Dynamic FEA Force vs Time curve of Multi-material t-1.5mm and l-3mm

6.2.5 Cell wall thickness 1.5 and cell size 3.5

From the figure 26 we can observe that the material experience a progressive failure. At 0.039kN in .007ms it is observed that there is a kink in the horizontal direction of the curve which shows that the elastomer is absorbing the velocity of the impactor at constant force. Then again the force experienced by the impactor increases to .0062kN in 0.04ms, the force from the elastomer is transferred to stiff material without much deflection. Then again the force experienced by the impactor increases to .0067kN and then the force gets decreased indicating the material has failed ultimately where in it is unable to resist the velocity of the impactor.

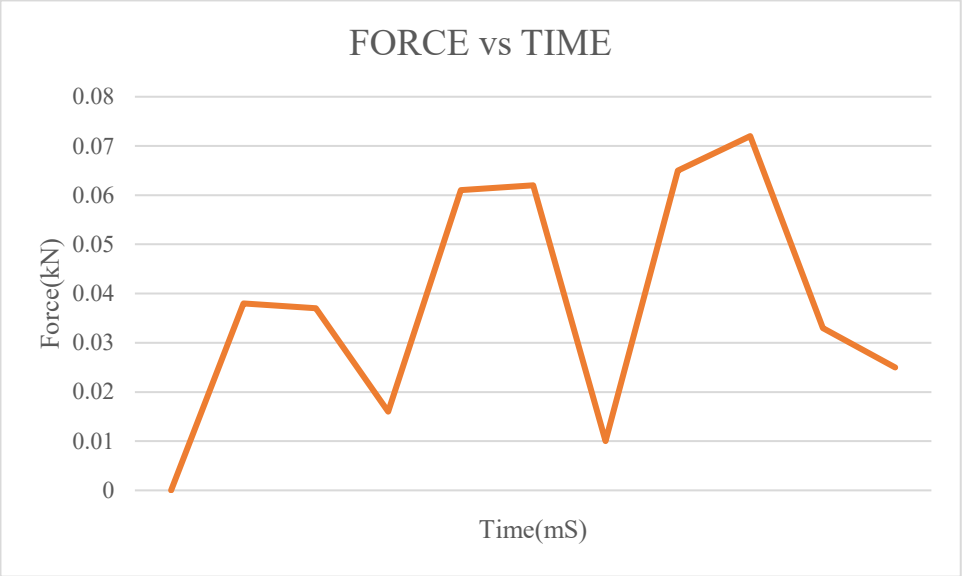

Figure 26. Dynamic FEA Force vs Time curve of Multi-material t-1.5mm and l-3.5mm

6.2.6 Cell wall thickness 2 and cell size 2.5

From the figure 27 we can observe that the material experience a progressive failure. At 0.2kN in .007ms it is observed that there is a kink in the horizontal direction of the curve which shows that the elastomer is absorbing the velocity of the impactor at constant force. Then again the force experienced by the impactor increases to 0.21kN in 0.015ms, the force from the elastomer is transferred to stiff material without much deflection. Then again the force experienced by the impactor increases to 0.23N and then the force gets decreased indicating the material has failed ultimately where in it is unable to resist the velocity of the impactor.

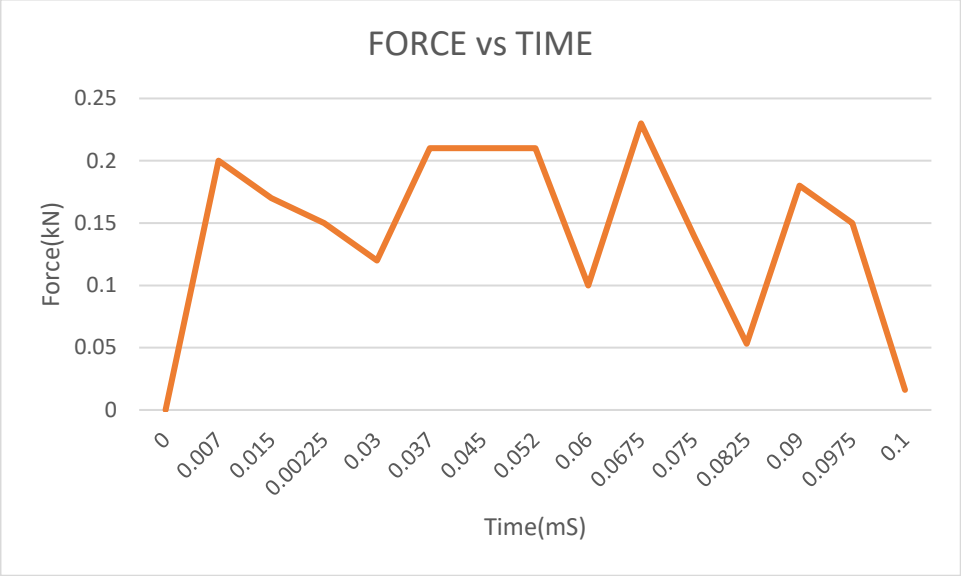

Figure 27. Dynamic FEA Force vs Time curve of Multi-material t-2mm and l-2.5mm

6.2.7 Cell wall thickness 2 and cell size 3

From the figure 28 we can observe that the material experience a progressive failure. At 0.17kN in .007ms it is observed that there is a kink in the horizontal direction of the curve which shows that the elastomer is absorbing the velocity of the impactor at constant force. Then again the force experienced by the impactor decreases to 0.16kN in 0.015ms, the force from the elastomer is transferred to stiff material without much deflection. Then again the force experienced by the impactor continues at 0.16kN and then the force gets decreased indicating the material has failed ultimately where in it is unable to resist the velocity of the impactor.

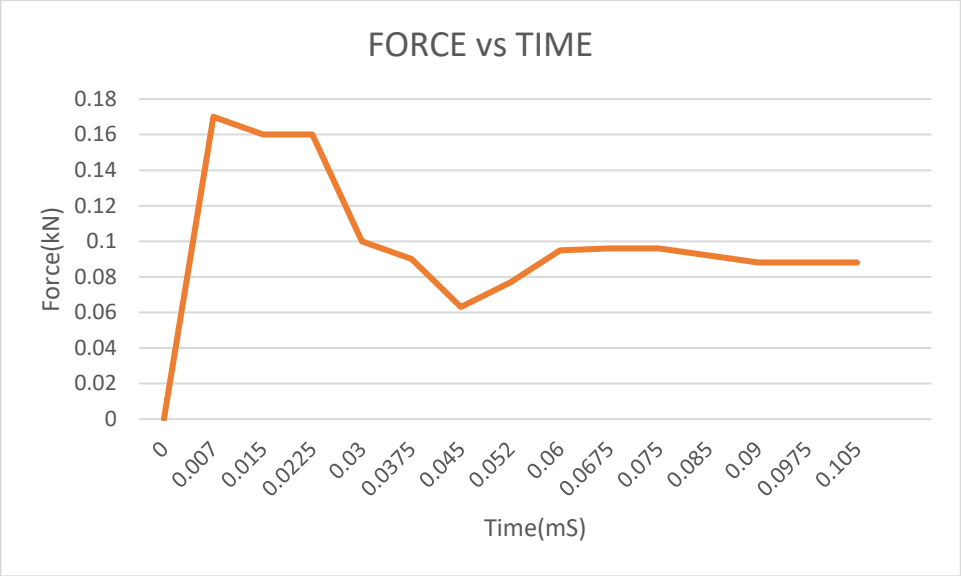

Figure 28: Dynamic FEA Force vs Time curve of Multi-material t-2mm and l-3mm

6.2.8 Cell wall thickness 2 and cell size 3.5

From the figure 29 we can observe that the material experience a progressive failure. At 0.165kN in .005ms it is observed that there is a kink in the horizontal direction of the curve which shows

that the elastomer is absorbing the velocity of the impactor at constant force. Then again the force experienced by the impactor increases to 0.29kN in 0.016ms, the force from the elastomer is transferred to stiff material without much deflection and then the force gets decreased indicating the material has failed ultimately where in it is unable to resist the velocity of the impactor.

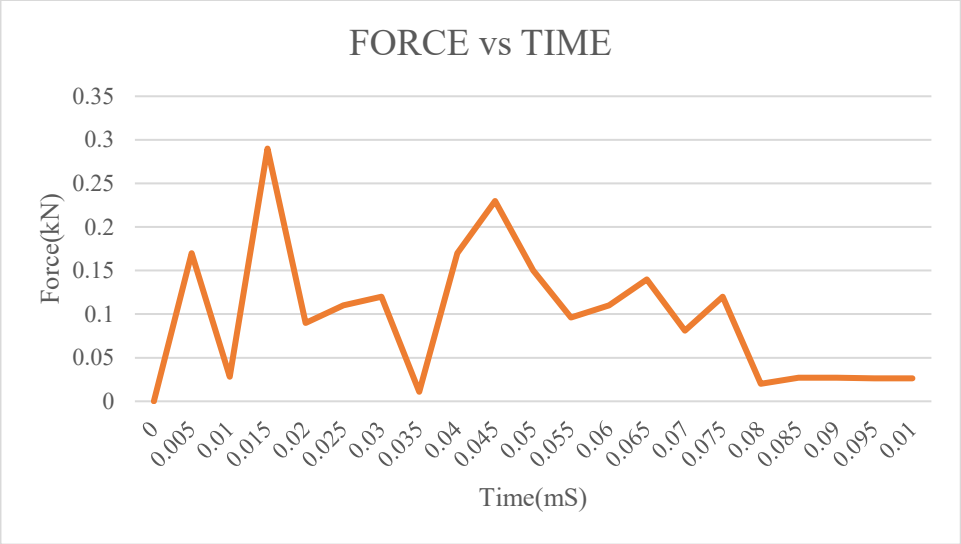

Figure 29. Dynamic FEA Force vs Time curve of Multi-material t-2mm and l-3.5mm

Table 2: Results of Dynamic FEA analysis of single and multi-material honeycomb structure

MODEL	ANALYTICAL FORCE (kN)
SINGLE MATERIAL T1, L2.5	2
MULTI-MATERIAL T1, L2.5	0.016
SINGLE MATERIAL T1, L3	1.5
MULTI-MATERIAL T1, L3	0.013
SINGLE MATERIAL T1, L3.5	1.5
MULTI-MATERIAL T1, L3.5	0.04
SINGLE MATERIAL T1.5, L2.5	4.25
MULTI-MATERIAL T1.5, L2.5	0.05
SINGLE MATERIAL T1.5, L3	3.75
MULTI-MATERIAL T1.5, L3	0.08
SINGLE MATERIAL T1.5, L3.5	3.5
MULTI-MATERIAL T1.5, L3.5	0.039
SINGLE MATERIAL T2, L2.5	3.5
MULTI-MATERIAL T2, L2.5	0.2
SINGLE MATERIAL T2, L3	2.5
MULTI-MATERIAL T2, L3	0.17
SINGLE MATERIAL T2, L3.5	0.09
MULTI-MATERIAL T2, L3.5	0.165

6.3 SINGLE MATERIAL STATIC FINITE ELEMENT ANALYSIS

This section involves the static FEA analysis of single material honeycomb structure with various cell wall thickness and cell wall size.

6.3.1 Cell wall thickness 1 and cell size 2.5

From the figure 30 we can observe that the material experience a steep failure. During compression the material reaches a maximum steep force of 4kN and then the force prolongs to stay in the same load indicating the inability of the material to absorb further force or energy, which is due to the stiffness of the material.

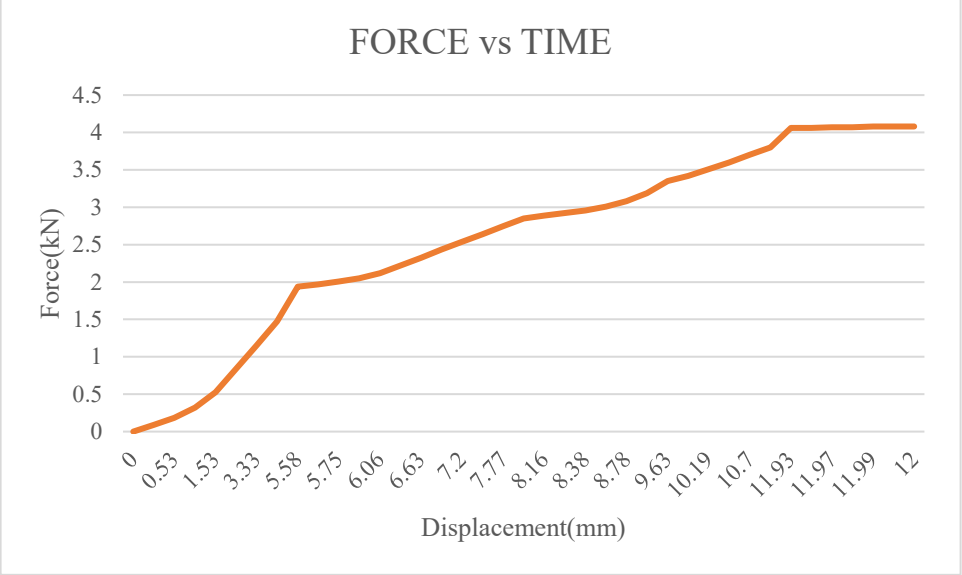

Figure 30. Static FEA Force vs Displacement curve of single material t-1mm and l-2.5mm

6.3.2 Cell wall thickness 1 and cell size 3

From the figure 31 we can observe that the material experience a steep failure. During compression the material reaches a maximum steep force of 3kN and then the force prolongs to stay in the same load indicating the inability of the material to absorb further force or energy, which is due to the stiffness of the material.

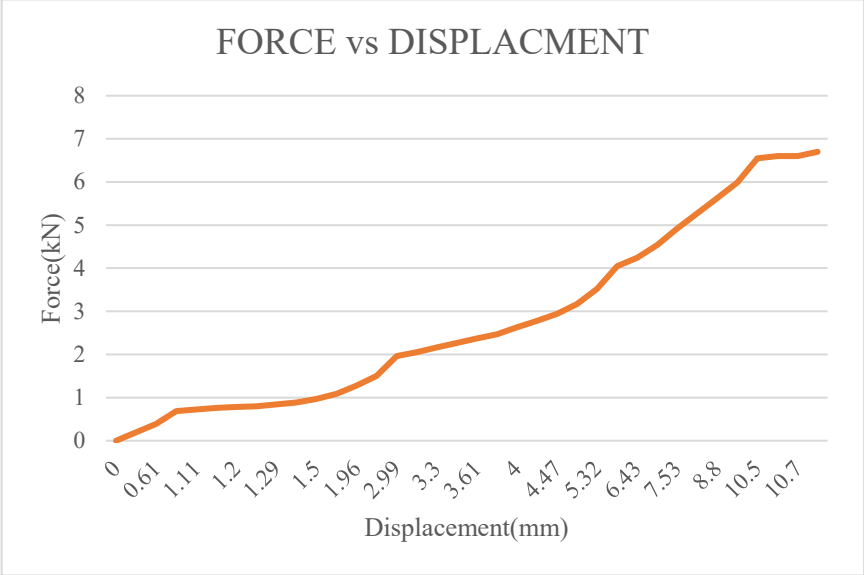

Figure 31. Static FEA Force vs Displacement curve of single material t-1mm and 3mm

6.3.3 Cell wall thickness 1 and cell size 3.5

From the figure 32 we can observe that the material experience a steep failure. During compression the material reaches a maximum steep force of 3.9kN and then the force prolongs to stay in the same load indicating the inability of the material to absorb further force or energy, which is due to the stiffness of the material.

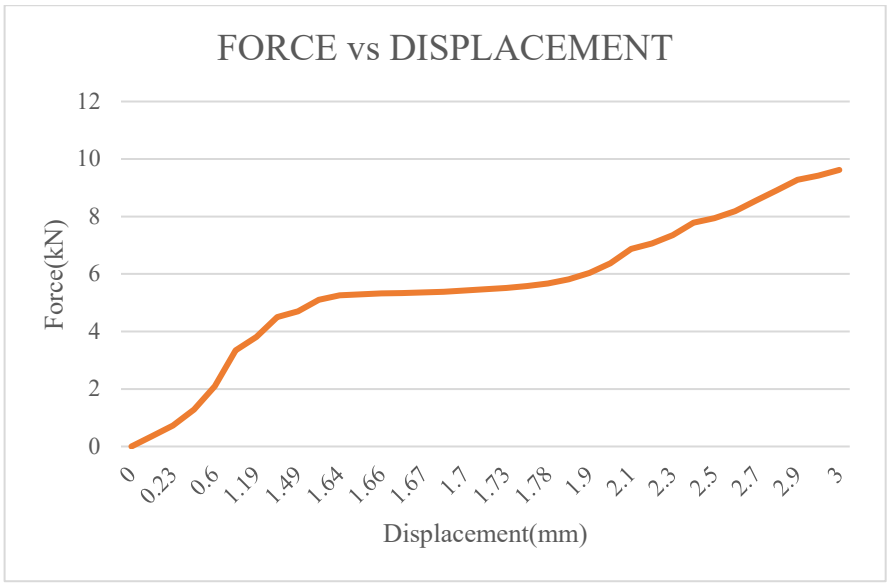

Figure 32. Static FEA Force vs Displacement curve of single material t-1mm and l-3.5mm

6.3.4 Cell wall thickness 1.5 and cell size 2.5

From the figure 33 we can observe that the material experience a steep failure. During compression the material reaches a maximum steep force of 10.5kN and then the force prolongs to stay in the same load indicating the inability of the material to absorb further force or energy, which is due to the stiffness of the material.

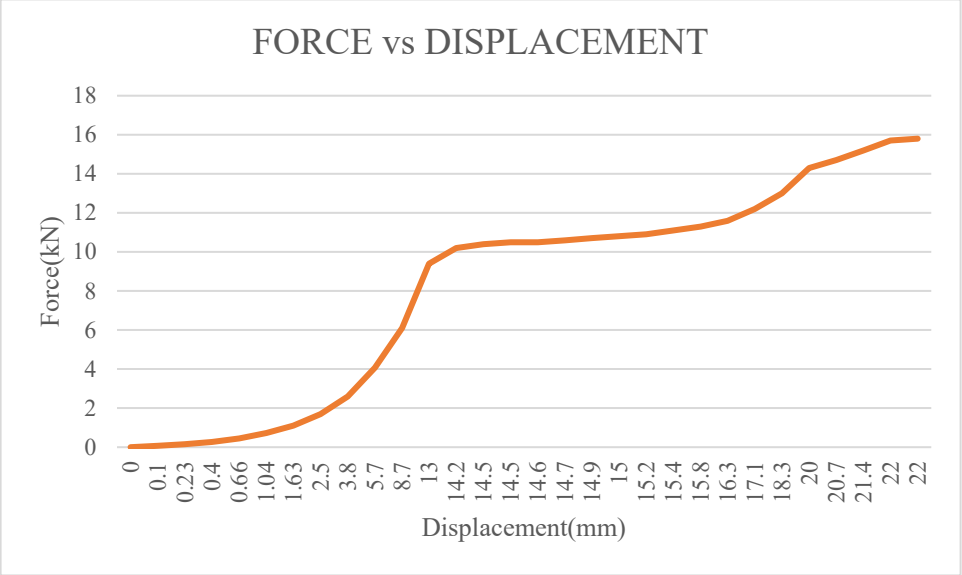

Figure 33. Static FEA Force vs Displacement curve of single material t-1.5mm and l-2.5mm

6.3.5 Cell wall thickness 1.5 and cell size 3

From the figure 34 we can observe that the material experience a steep failure. During compression the material reaches a maximum steep force of 9.9kN and then the force prolongs to stay in the same load indicating the inability of the material to absorb further force or energy, which is due to the stiffness of the material.

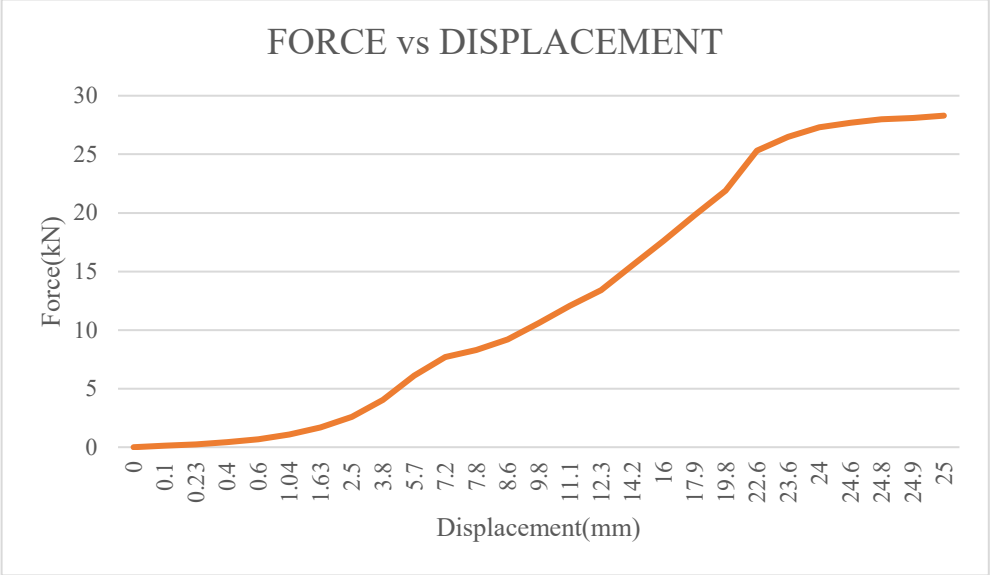

Figure 34. Static FEA Force vs Displacement curve of single material t-1.5mm and l-3mm

6.3.6 Cell wall thickness 1.5 and cell size 3.5

From the figure 35 we can observe that the material experience a steep failure. During compression the material reaches a maximum steep force of 7.5kN and then the force prolongs to stay in the same load indicating the inability of the material to absorb further force or energy, which is due to the stiffness of the material.

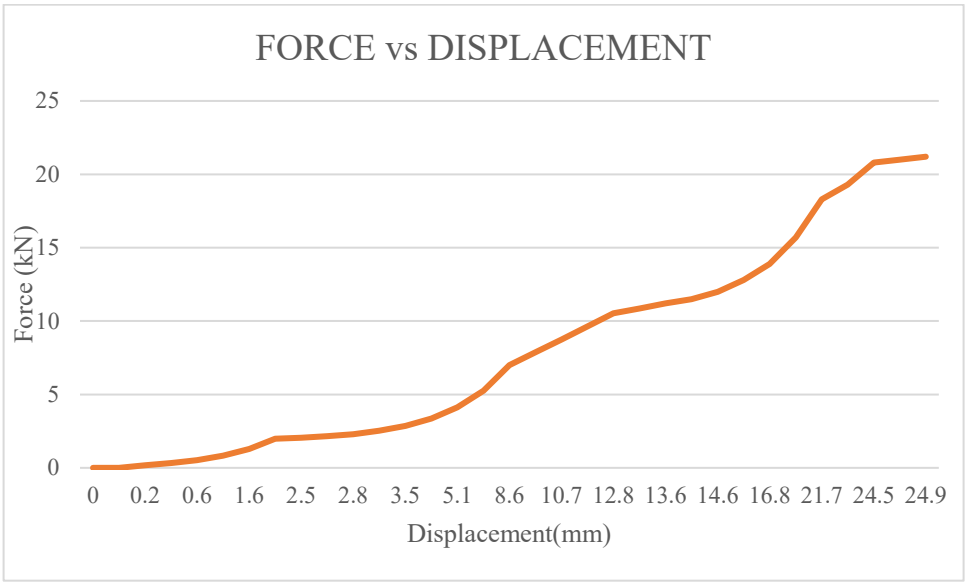

Figure 35. Static FEA Force vs Displacement curve of single material t-1.5mm and l-3.5mm

6.3.7 Cell wall thickness 2 and cell size 2.5

From the figure 36 we can observe that the material experience a steep failure. During compression the material reaches a maximum steep force of 15kN and then the force prolongs to stay in the same load

indicating the inability of the material to absorb further force or energy, which is due to the stiffness of the material.

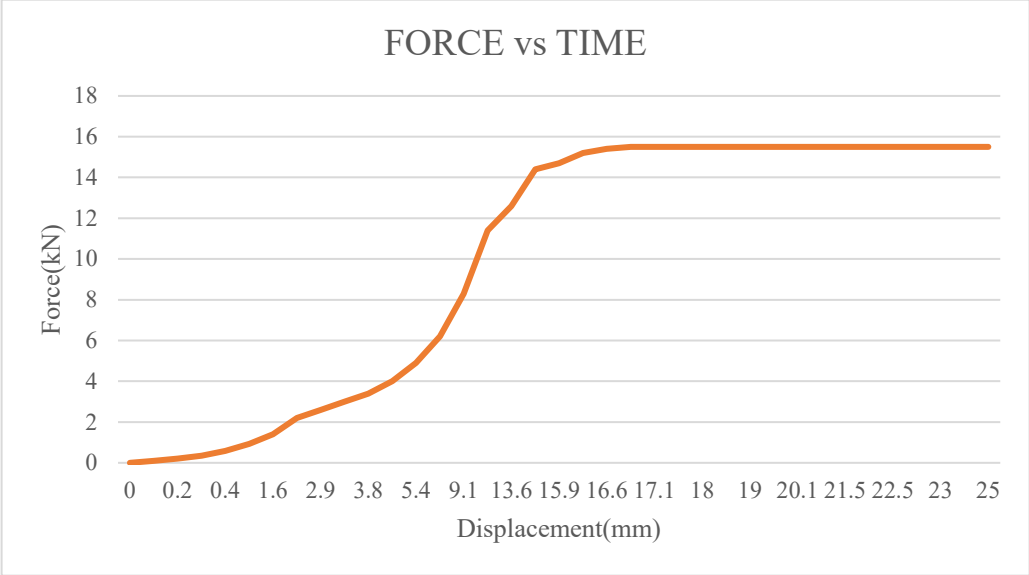

Figure 36. Static FEA Force vs Displacement curve of single material t-2mm and 2.5mm

6.3.8 Cell wall thickness 2 and cell size 3

From the figure 37 we can observe that the material experience a steep failure. During compression the material reaches a maximum steep force of 12.5kN and then the force prolongs to stay in the same load indicating the inability of the material to absorb further force or energy, which is due to the stiffness of the material.

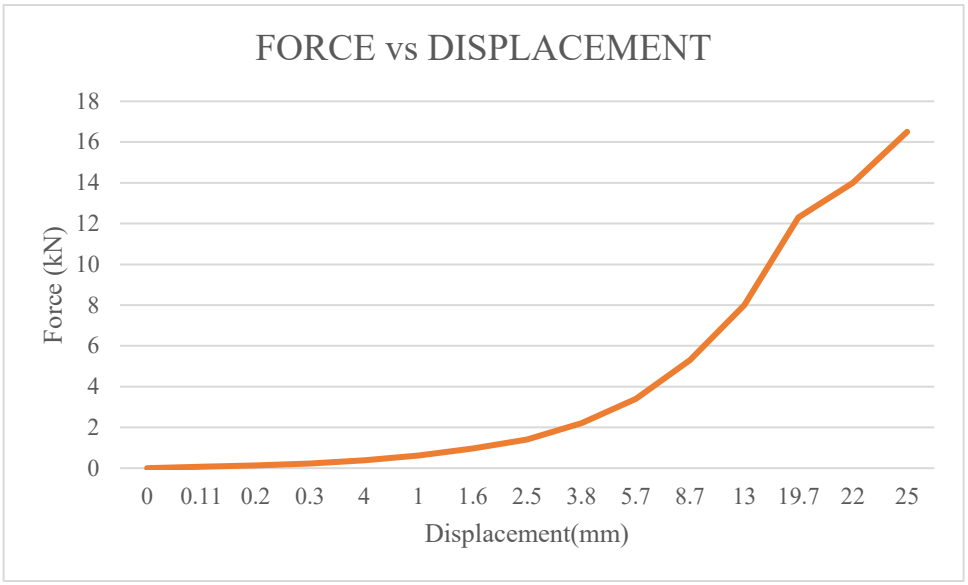

Figure 37. Static FEA Force vs Displacement curve of single material t-2mm and l-3mm

6.3.9 Cell wall thickness 2 and cell size 3.5

From the figure 38 we can observe that the material experience a steep failure. During compression the material reaches a maximum steep force of 12kN and then the force prolongs to stay in the same load indicating the inability of the material to absorb further force or energy, which is due to the stiffness of the material.

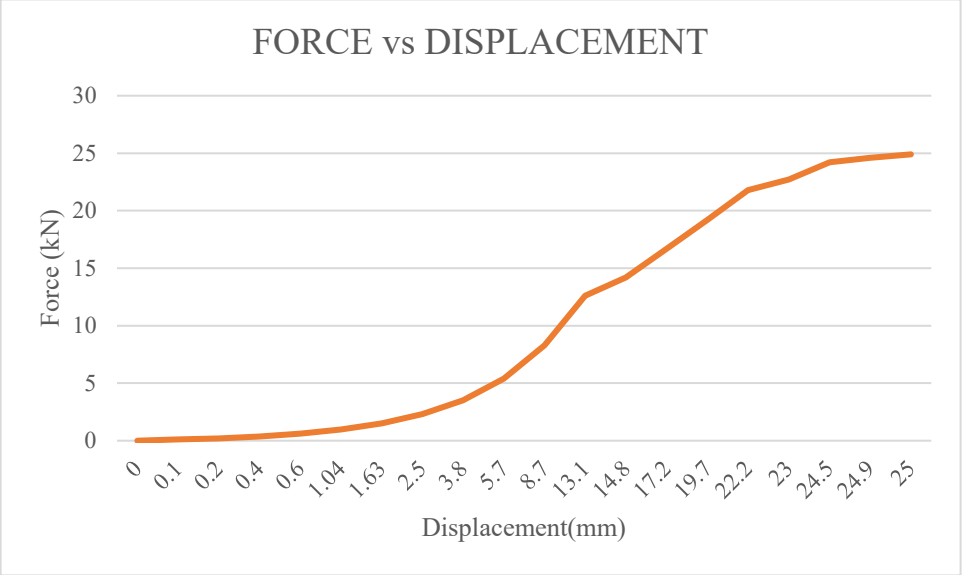

Figure 38. Static FEA Force vs Displacement curve of single material t-2mm and l-3.5mm

6.4 MULTI-MATERIAL STATIC FINITE ELEMENT ANALYSIS

This section involves the static FEA analysis of multi-material honeycomb structure with various cell wall thickness and cell wall size.

6.4.1 Cell wall thickness 1 and cell size 2.5

From the figure 39 we can observe that the material experiences a progressive failure. During compression the material reaches a force of 5kN and it produces a kink and then the force reaches up to 8kN with another kink and finally reaches 12kN and prolongs to stay in the same load indicating the inability of the material to absorb further force or energy, which is due to the stiffness of the material.

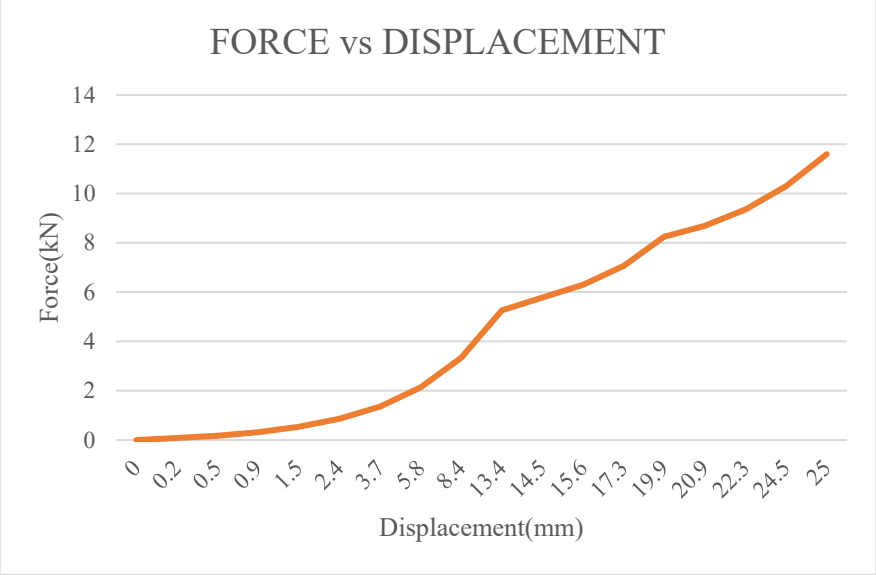

Figure 39. Static FEA Force vs Displacement curve of Multi-material t-1mm and l-2.5mm

6.4.2 Cell wall thickness 1 and cell size 3

From the figure 40 we can observe that the material experiences a progressive failure. During compression the material reaches a force of 3kN and it produces a kink and then the force reaches up to 5kN with another kink and finally reaches 7kN and prolongs to stay in the same load indicating the inability of the material to absorb further force or energy, which is due to the stiffness of the material.

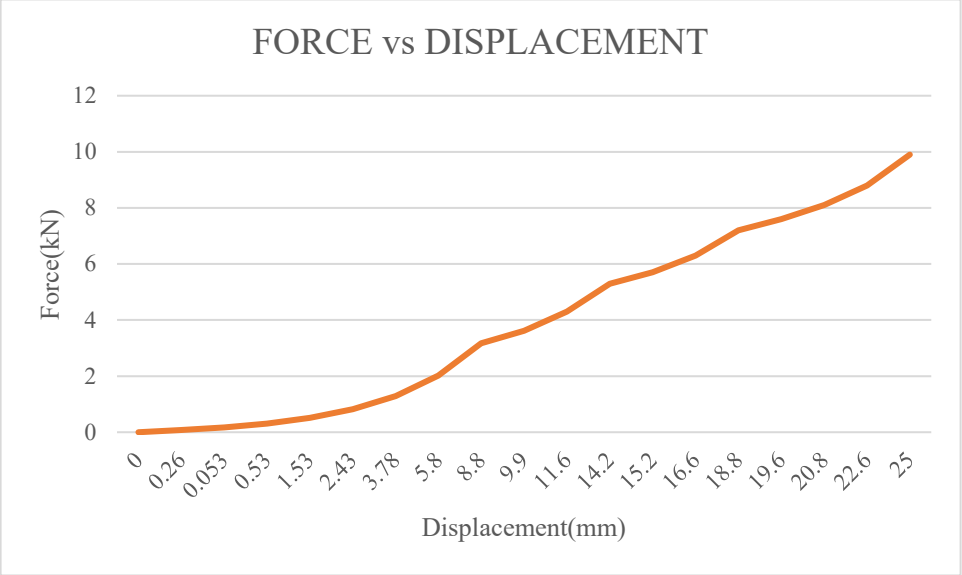

Figure 40. Static FEA Force vs Displacement curve of Multi-material t-1mm and 3mm

6.4.3 Cell wall thickness 1 and cell size 3.5

From the figure 41 we can observe that the material experiences a progressive failure. During compression the material reaches a force of 2.5kN and it produces a kink and then the force reaches up to 5kN with another kink and finally reaches 8.5kN and prolongs to stay in the same load indicating the inability of the material to absorb further force or energy, which is due to the stiffness of the material.

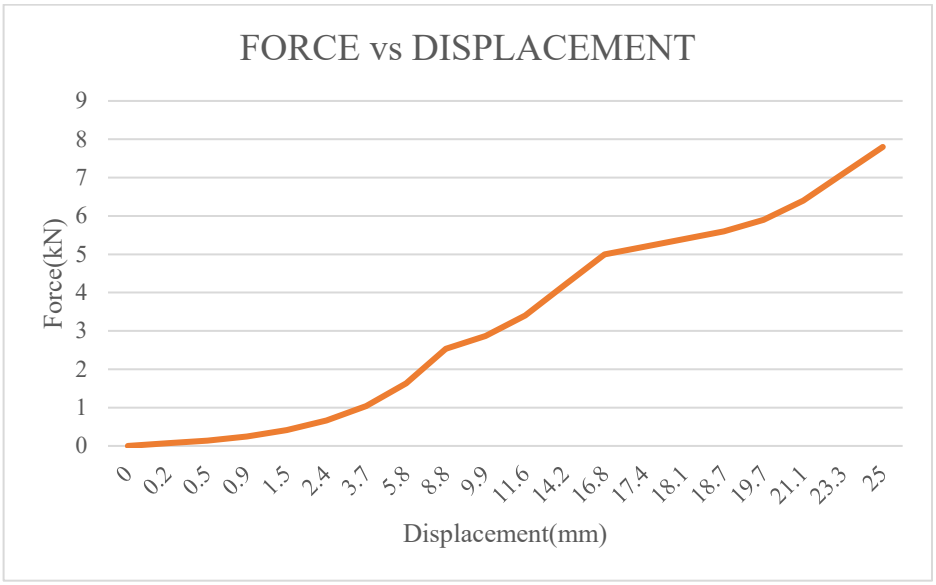

Figure 41. Static FEA Force vs Displacement curve of Multi-material t-1mm and l-3.5mm

6.4.4 Cell wall thickness 1.5 and cell size 2.5

From the figure 42 we can observe that the material experiences a progressive failure. During compression the material reaches a force of 3kN and it produces a kink and then the force reaches up to

4.5kN with another kink and finally reaches 5.88kN and prolongs to stay in the same load indicating the inability of the material to absorb further force or energy, which is due to the stiffness of the material.

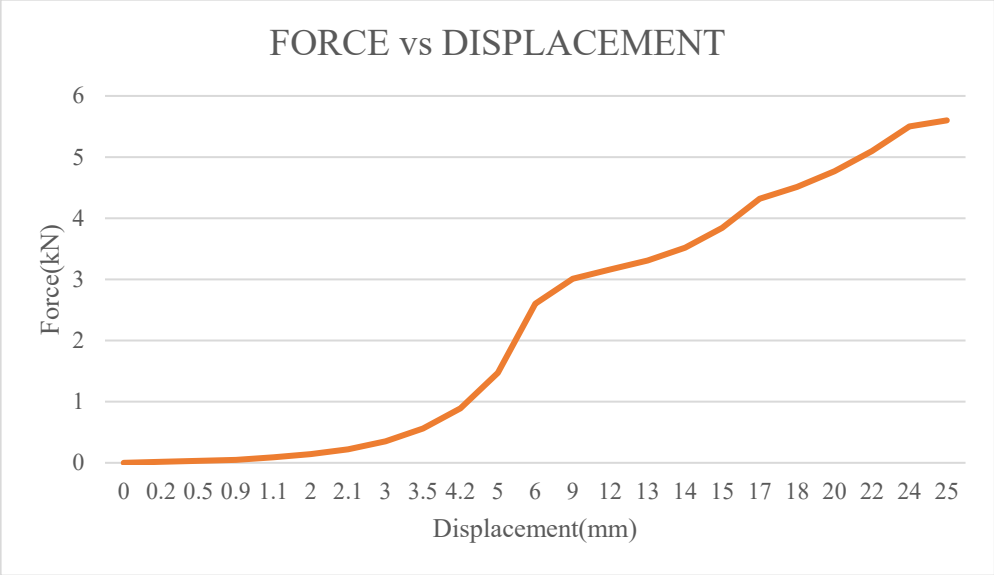

Figure 42. Static FEA Force vs Displacement curve of Multi-material t-1.5mm and l-2.5mm

6.4.5 Cell wall thickness 1.5 and cell size 3

From the figure 43 we can observe that the material experiences a progressive failure. During compression the material reaches a force of 1.4kN and it produces a kink and then the force reaches up to 2kN with another kink and finally reaches 2.4kN and prolongs to stay in the same load indicating the inability of the material to absorb further force or energy, which is due to the stiffness of the material.

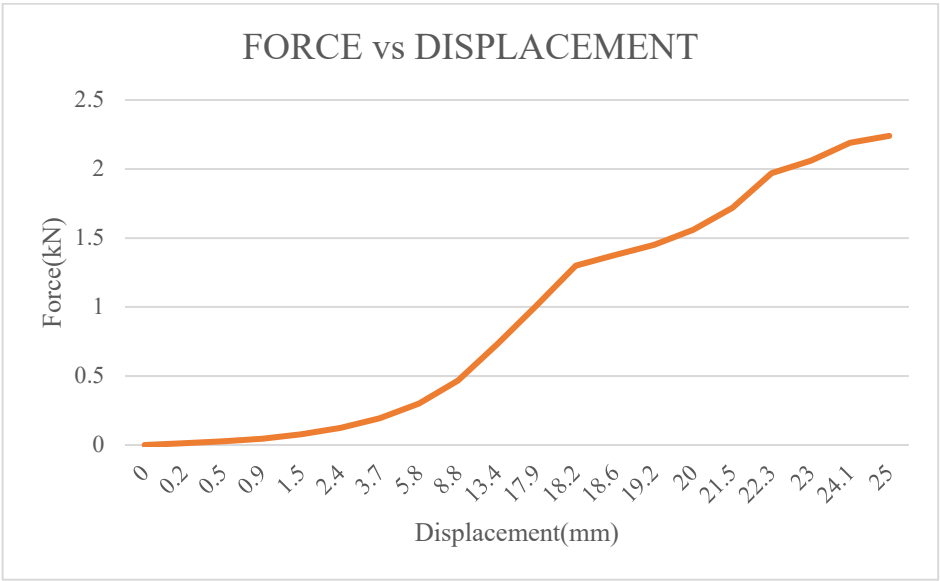

Figure 43. Static FEA Force vs Displacement curve of Multi-material t-1.5mm and l-3mm

6.4.6 Cell wall thickness 1.5 and cell size 3.5

From the figure 44 we can observe that the material experiences a progressive failure. During compression the material reaches a force of 0.9kN and it produces a kink and then the force reaches up to 1.75kN with another kink and finally reaches 1.9kN and prolongs to stay in the same load indicating the inability of the material to absorb further force or energy, which is due to the stiffness of the material.

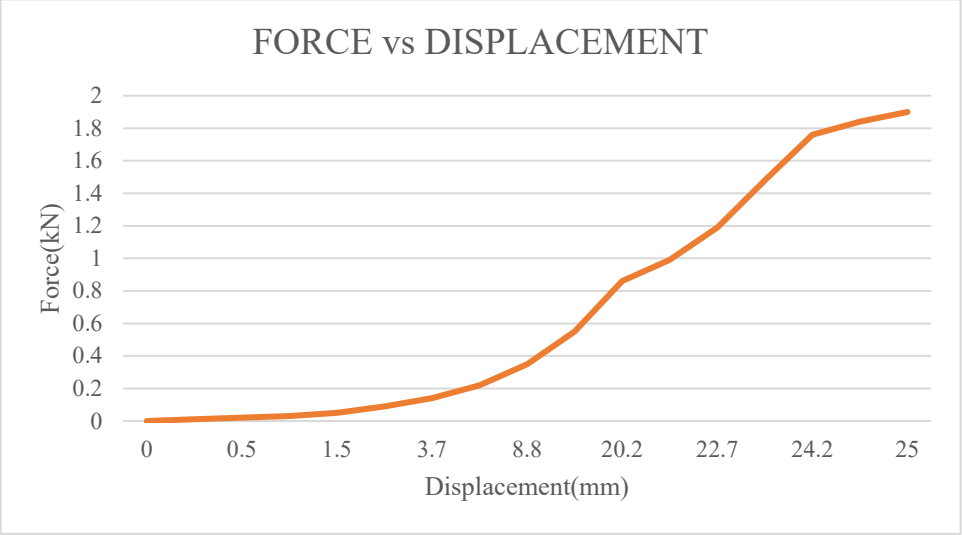

Figure 44. Static FEA Force vs Displacement curve of Multi-material t-1.5mm and l-3.5mm

6.4.7 Cell wall thickness 2 and cell size 2.5

From the figure 45 we can observe that the material experiences a progressive failure. During compression the material reaches a force of 7.5kN and it produces a kink and then the force reaches up to 13kN with another kink and finally reaches 20kN and prolongs to stay in the same load indicating the inability of the material to absorb further force or energy, which is due to the stiffness of the material.

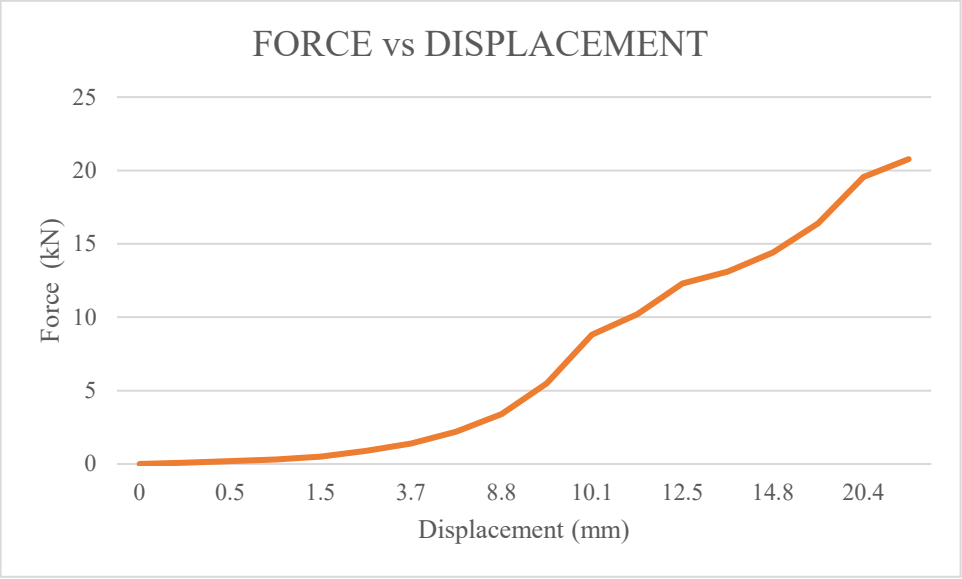

Figure 45. Static FEA Force vs Displacement curve of Multi-material t-2mm and 2.5mm

6.4.8 Cell wall thickness 2 and cell size 3

From the figure 46 we can observe that the material experiences a progressive failure. During compression the material reaches a force of 4kN and it produces a kink and then the force reaches up to 7kN with another kink and finally reaches 9kN and prolongs to stay in the same load indicating the inability of the material to absorb further force or energy, which is due to the stiffness of the material.

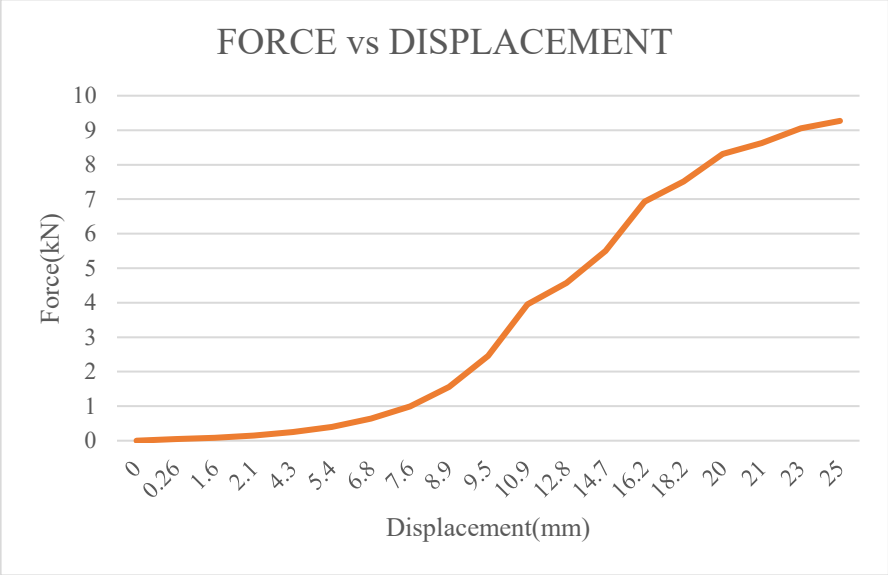

Figure 46. Static FEA Force vs Displacement curve of Multi-material t-2mm and l-3mm

6.4.9 Cell wall thickness 2 and cell size 3.5

From the figure 47 we can observe that the material experiences a progressive failure. During compression the material reaches a force of 1.9kN and it produces a kink and then the force reaches up to 3kN with another kink and finally reaches 3.25kN and prolongs to stay in the same load indicating the inability of the material to absorb further force or energy, which is due to the stiffness of the material.

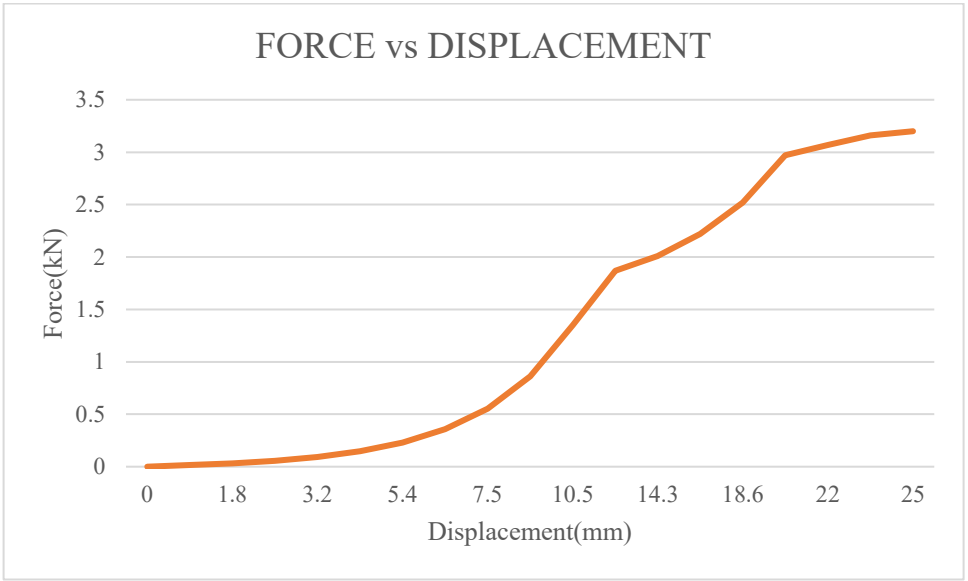

Figure 47. Static FEA Force vs Displacement curve of Multi-material t-2mm and l-3.5mm

6.5 SINGLE MATERIAL STATIC TESTING EXPERIMENTAL RESULTS

This section involves the static experimental analysis of single material honeycomb structure with various cell wall thickness and cell wall size.

6.5.1 Cell wall thickness 1 and cell size 2.5

From the figure 48 we can observe that the material experience a steep failure. During compression initially the top flat surface of the compression test rig is offset to certain distance before starting the compression, so the actual value of the compressive force on the material reaches a maximum steep force of 4.9kN and then the force prolongs to stay in the same load indicating the inability of the material to absorb further force or energy, which is due to the stiffness of the material.

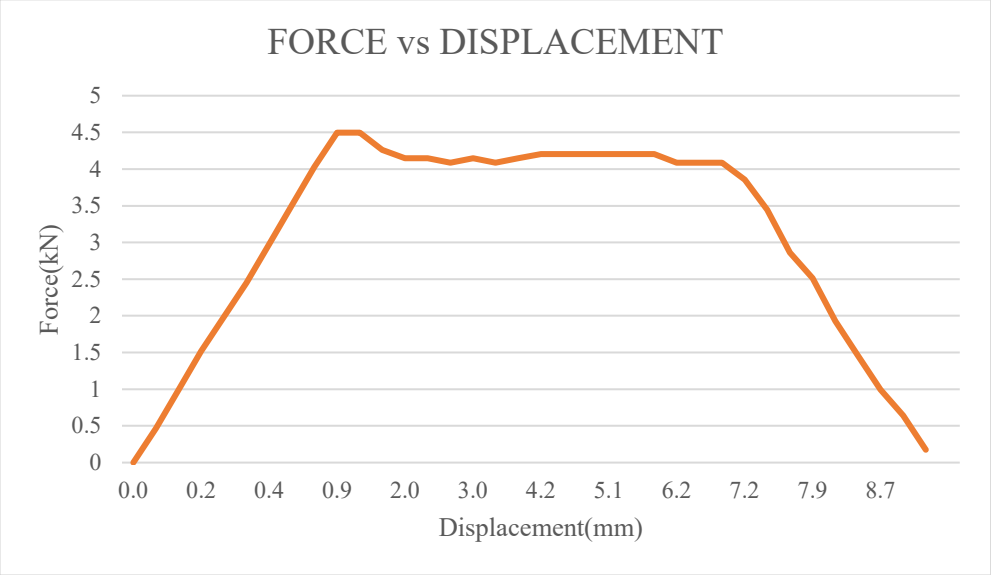

Figure 48. Static Experimental Force vs Displacement curve of single material t-1mm and l-2.5mm

6.5.2 Cell wall thickness 1 and cell size 3

From the figure 49 we can observe that the material experience a steep failure. During compression the material reaches a maximum steep force of 4.9kN and then the force prolongs to stay in the same load indicating the inability of the material to absorb further force or energy, which is due to the stiffness of the material.

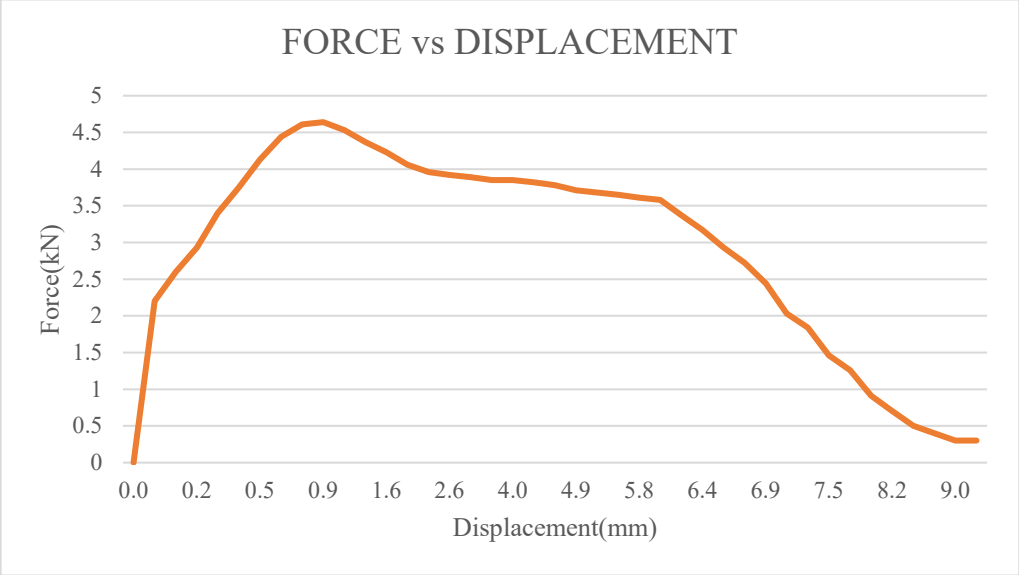

Figure 49. Static Experimental Force vs Displacement curve of single material t-1mm and 3mm

6.5.3 Cell wall thickness 1 and cell size 3.5

From the figure 50 we can observe that the material experience a steep failure. During compression the material reaches a maximum steep force of 4.5kN and then the force prolongs to stay in the same load indicating the inability of the material to absorb further force or energy, which is due to the stiffness of the material.

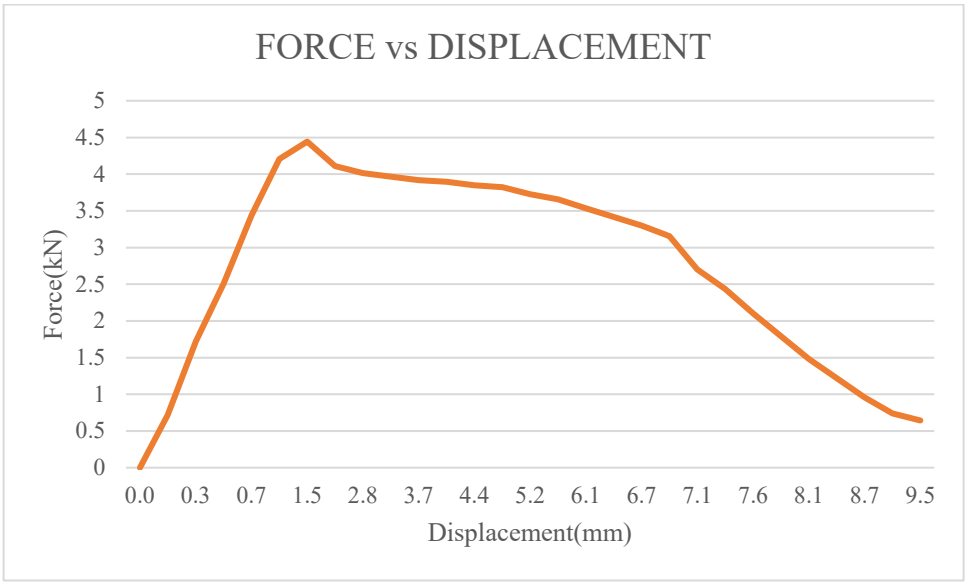

Figure 50. Static Experimental Force vs Displacement curve of single material t-1mm and l-3.5mm

6.5.4 Cell wall thickness 1.5 and cell size 2.5

From the figure 51 we can observe that the material experience a steep failure. During compression the material reaches a maximum steep force of 10kN and then the force prolongs to stay in the same load

indicating the inability of the material to absorb further force or energy, which is due to the stiffness of the material.

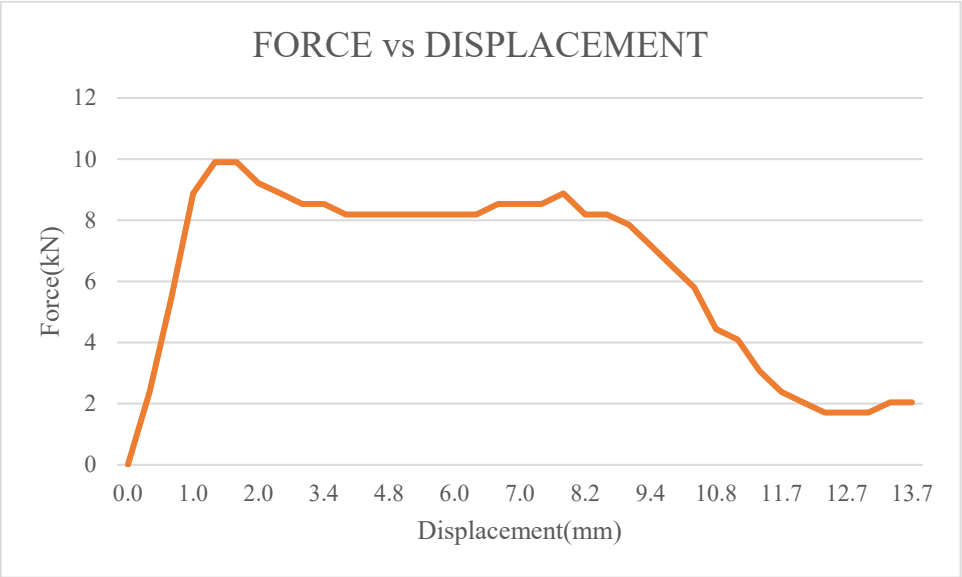

Figure 51. Static Experimental Force vs Displacement curve of single material t-1.5mm and l-2.5mm

6.5.5 Cell wall thickness 1.5 and cell size 3

From the figure 52 we can observe that the material experience a steep failure. During compression the material reaches a maximum steep force of 8kN and then the force prolongs to stay in the same load indicating the inability of the material to absorb further force or energy, which is due to the stiffness of the material.

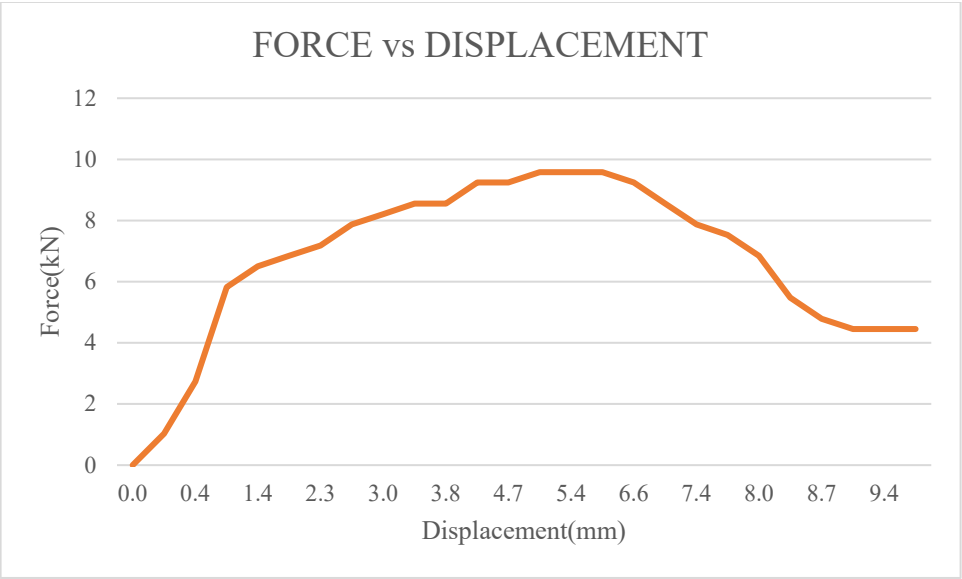

Figure 52. Static Experimental Force vs Displacement curve of single material t-1.5mm and l-3mm

6.5.6 Cell wall thickness 1.5 and cell size 3.5

From the figure 53 we can observe that the material experience a steep failure. During compression the material reaches a maximum steep force of 7.4kN and then the force prolongs to stay in the same load indicating the inability of the material to absorb further force or energy, which is due to the stiffness of the material.

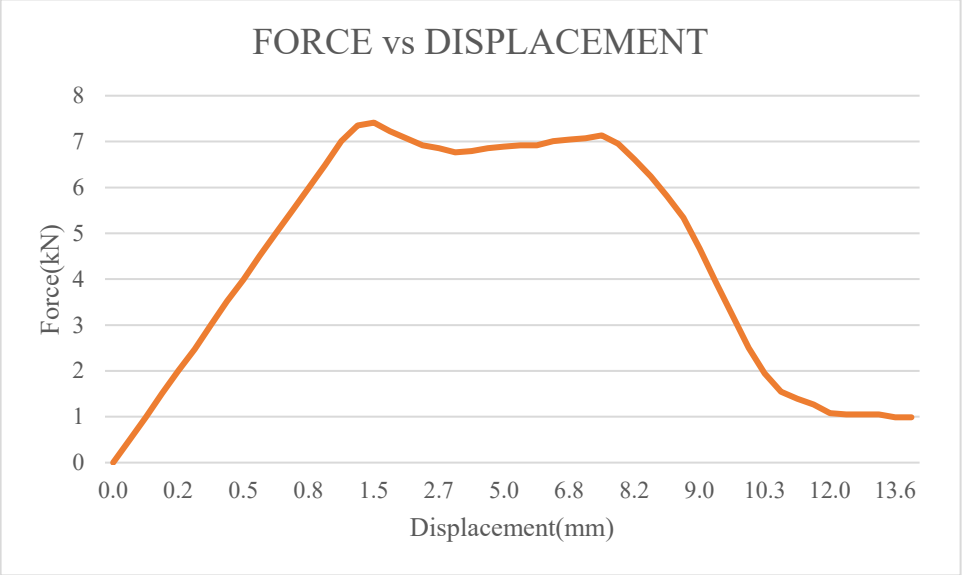

Figure 53. Static Experimental Force vs Displacement curve of single material t-1.5mm and l-3.5mm

6.5.7 Cell wall thickness 2 and cell size 2.5

From the figure 54 we can observe that the material experience a steep failure. During compression the material reaches a maximum steep force of 15kN and then the force prolongs to stay in the same load indicating the inability of the material to absorb further force or energy, which is due to the stiffness of the material.

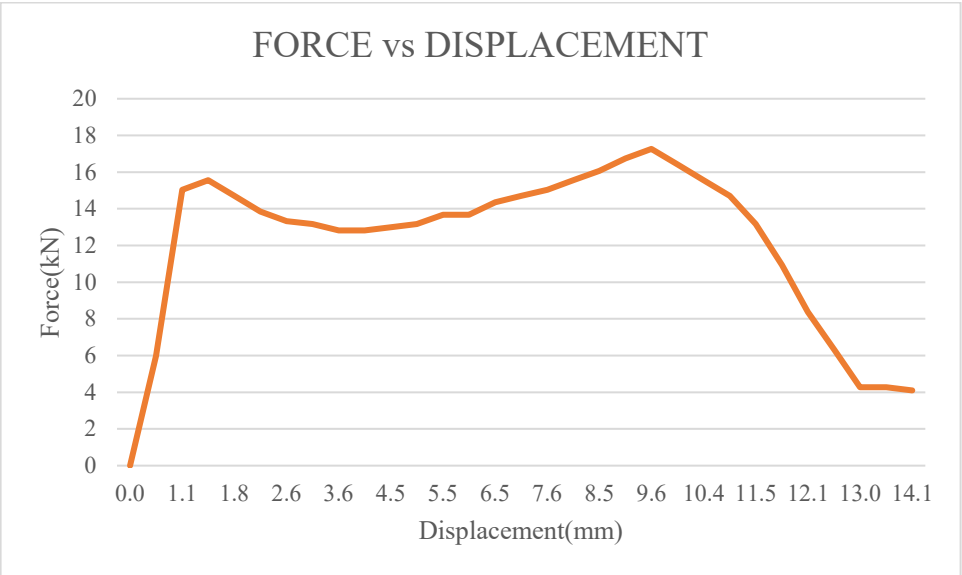

Figure 54. Static Experimental Force vs Displacement curve of single material t-2mm and 2.5mm

6.5.8 Cell wall thickness 2 and cell size 3

From the figure 55 we can observe that the material experience a steep failure. During compression the material reaches a maximum steep force of 12kN and then the force prolongs to stay in the same load indicating the inability of the material to absorb further force or energy, which is due to the stiffness of the material.

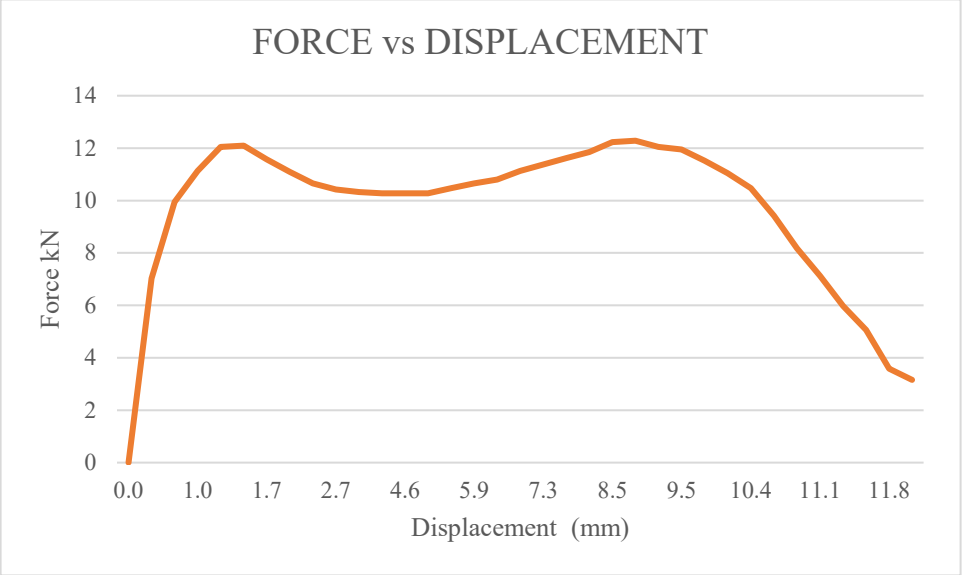

Figure 55. Static Experimental Force vs Displacement curve of single material t-2mm and l-3mm

6.5.9 Cell wall thickness 2 and cell size 3.5

From the figure 56 we can observe that the material experience a steep failure. During compression the material reaches a maximum steep force of 10kN and then the force prolongs to stay in the same load indicating the inability of the material to absorb further force or energy, which is due to the stiffness of the material.

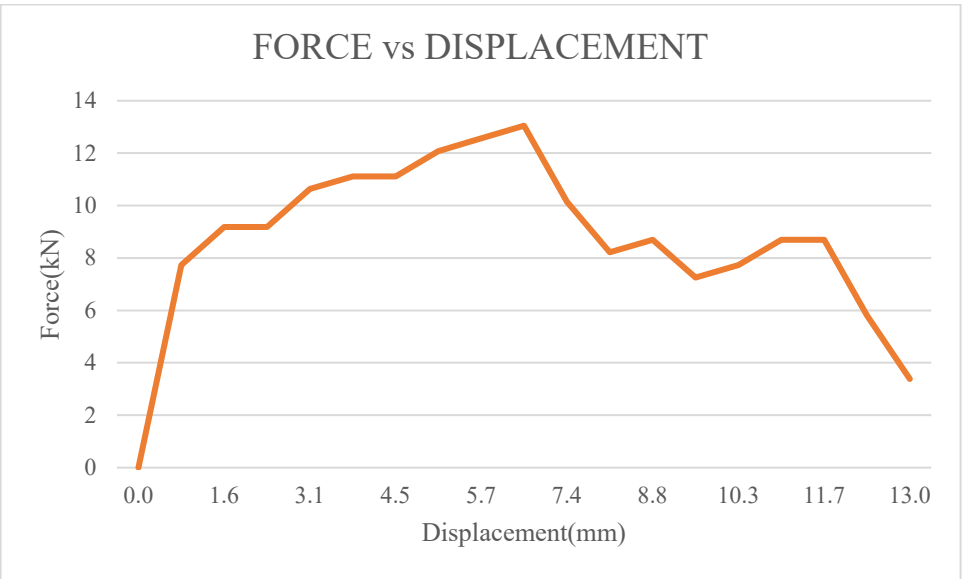

Figure 56. Static Experimental Force vs Displacement curve of single material t-2mm and l-3.5mm

6.6 MULTI-MATERIAL STATIC EXPERIMENTAL RESULTS

This section involves the static experimental analysis of multi-material honeycomb structure with various cell wall thickness and cell wall size.

6.6.1 Cell wall thickness 1 and cell size 2.5

From the figure 57 we can observe that the material experiences a progressive failure. During compression the material reaches a force of 3.4kN and it produces a kink and then the force reaches up to 5kN with another kink and finally reaches 10kN and increases steeply indicating the inability of the material to absorb further force or energy, which is due to the stiffness of the material.

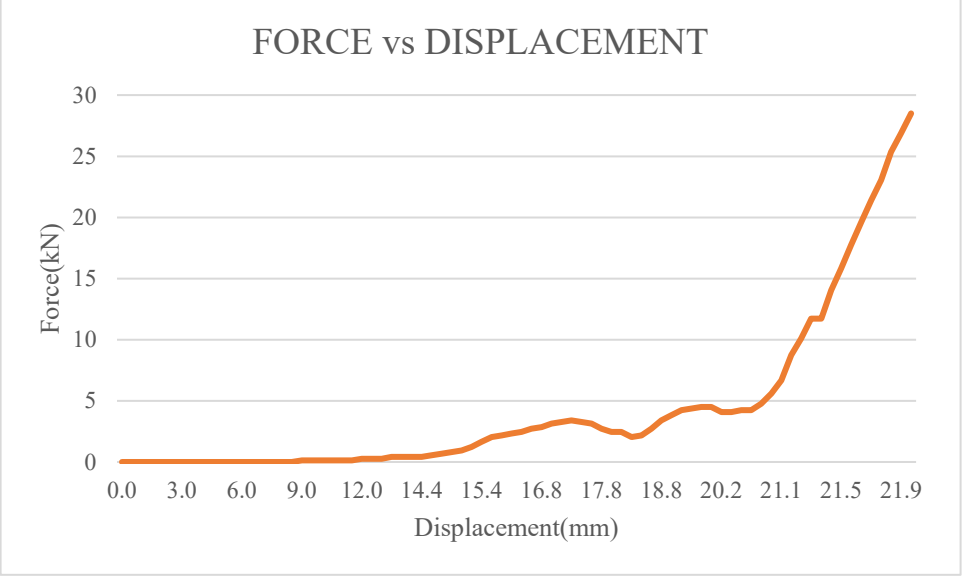

Figure 57. Static Experimental Force vs Displacement curve of Multi-material t-1mm and l-2.5mm

6.6.2 Cell wall thickness 1 and cell size 3

From the figure 58 we can observe that the material experiences a progressive failure. During compression the material reaches a force of 2kN and it produces a kink and then the force reaches up to 2.5kN with another kink and finally reaches 2.7kN and increases steeply indicating the inability of the material to absorb further force or energy, which is due to the stiffness of the material.

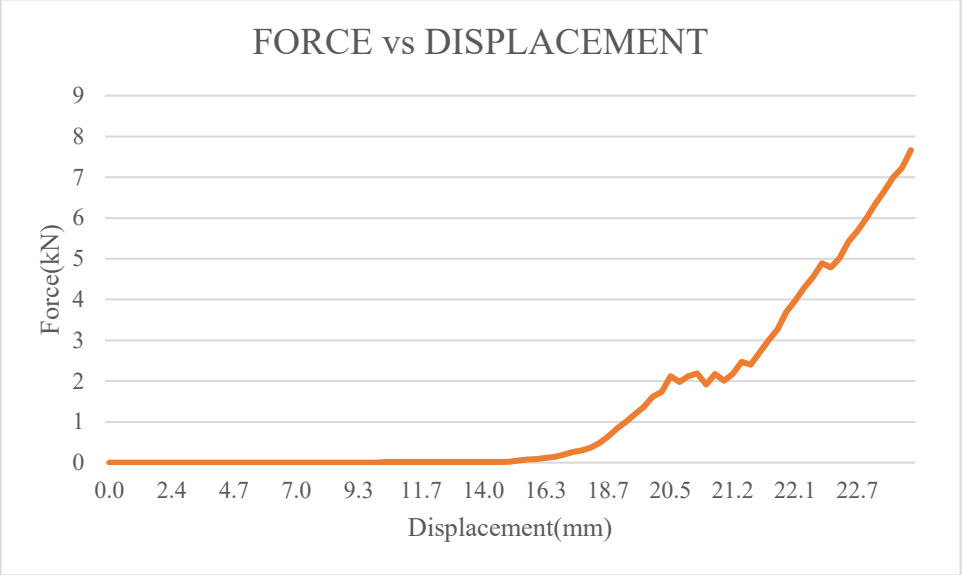

Figure 58. Static Experimental Force vs Displacement curve of Multi-material t-1mm and 3mm

6.6.3 Cell wall thickness 1 and cell size 3.5

From the figure 59 we can observe that the material experiences a progressive failure. During compression the material reaches a force of 0.9kN and it produces a kink and then the force reaches up to 1kN with another kink and finally reaches 1.5kN and increases steeply indicating the inability of the material to absorb further force or energy, which is due to the stiffness of the material.

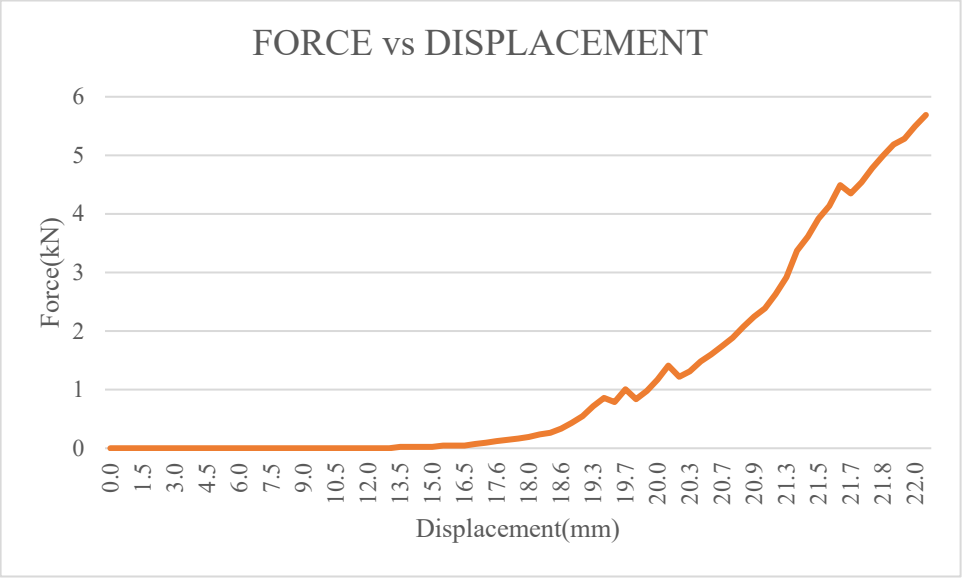

Figure 59. Static Experimental Force vs Displacement curve of Multi-material t-1mm and l-3.5mm

6.6.4 Cell wall thickness 1.5 and cell size 2.5

From the figure 60 we can observe that the material experiences a progressive failure. During compression the material reaches a force of 5kN and it produces a kink and then the force reaches up to 8kN

with another kink and finally reaches 10kN and increases steeply indicating the inability of the material to absorb further force or energy, which is due to the stiffness of the material.

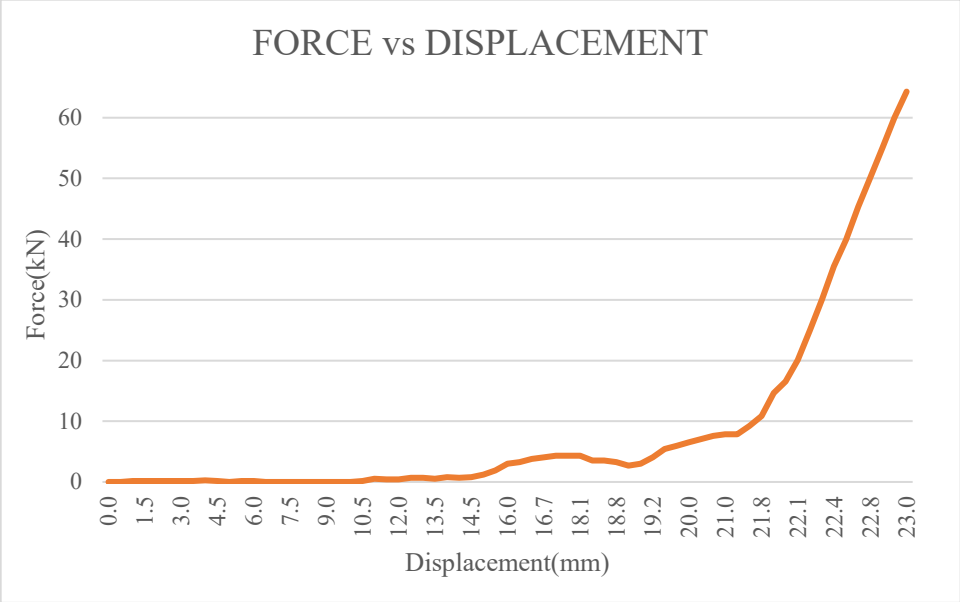

Figure 60. Static Experimental Force vs Displacement curve of Multi-material t-1.5mm and l-2.5mm

6.6.5 Cell wall thickness 1.5 and cell size 3

From the figure 61 we can observe that the material experiences a progressive failure. During compression the material reaches a force of 3.9kN and it produces a kink and then the force reaches up to 4.5kN with another kink and finally reaches 6kN and increases steeply indicating the inability of the material to absorb further force or energy, which is due to the stiffness of the material.

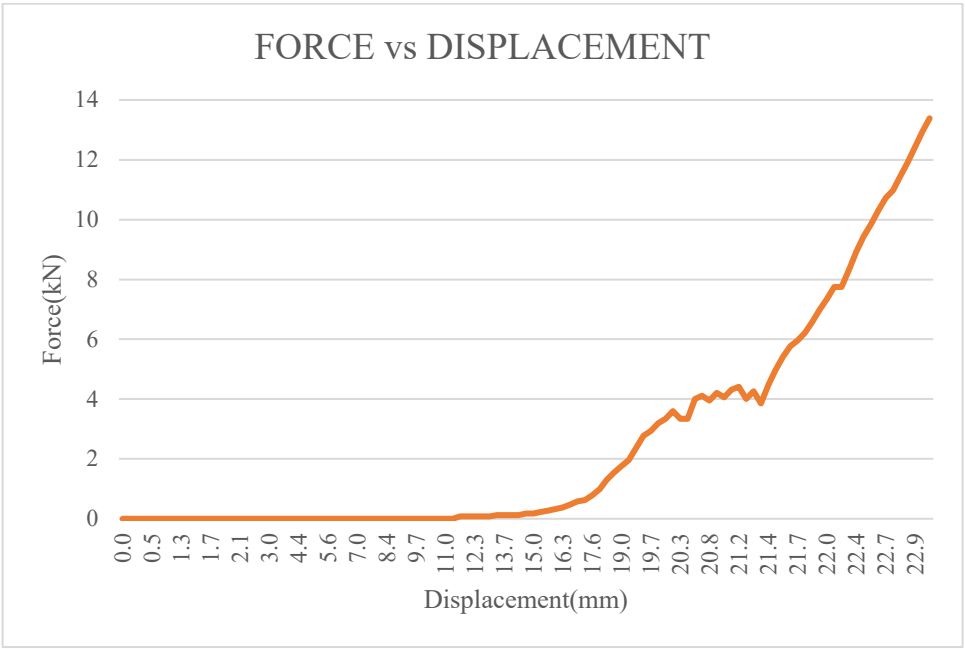

Figure 61. Static Experimental Force vs Displacement curve of Multi-material t-1.5mm and l-3mm

6.6.6 Cell wall thickness 1.5 and cell size 3.5

From the figure 62 we can observe that the material experiences a progressive failure. During compression the material reaches a force of 1kN and it produces a kink and then the force reaches up to 1.5kN with another kink and finally reaches 1.9kN and increases steeply indicating the inability of the material to absorb further force or energy, which is due to the stiffness of the material.

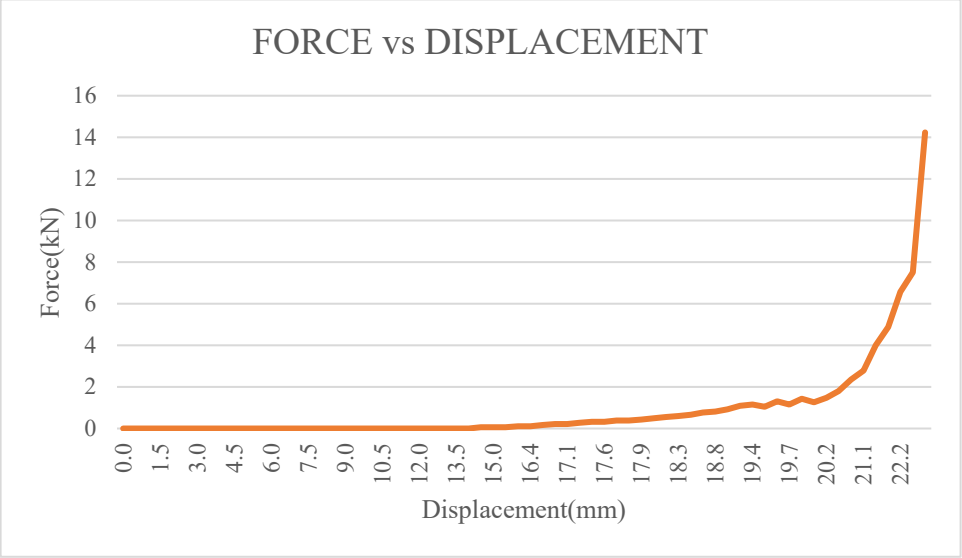

Figure 62. Static Experimental Force vs Displacement curve of Multi-material t-1.5mm and l-3.5mm

6.6.7 Cell wall thickness 2 and cell size 2.5

From the figure 63 we can observe that the material experiences a progressive failure. During compression the material reaches a force of 4.5kN and it produces a kink and then the force reaches up to 4.9kN with another kink and finally reaches 5kN and increases steeply indicating the inability of the material to absorb further force or energy, which is due to the stiffness of the material.

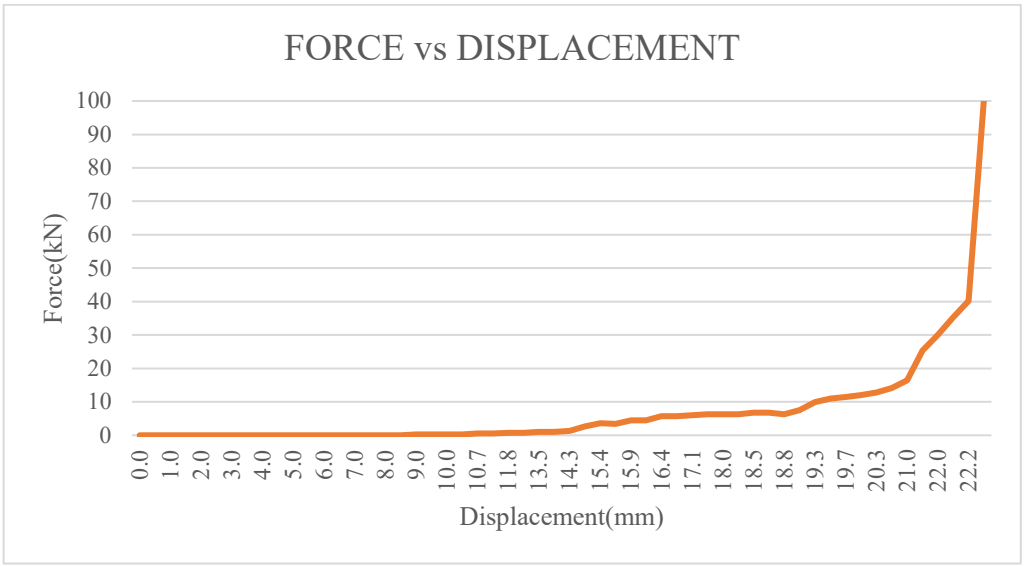

Figure 63. Static Experimental Force vs Displacement curve of Multi-material t-2mm and 2.5mm

6.6.8 Cell wall thickness 2 and cell size 3

From the figure 64 we can observe that the material experiences a progressive failure. During compression the material reaches a force of 4.1kN and it produces a kink and then the force reaches up to 4.2kN with another kink and finally reaches 4.4kN and increases steeply indicating the inability of the material to absorb further force or energy, which is due to the stiffness of the material.

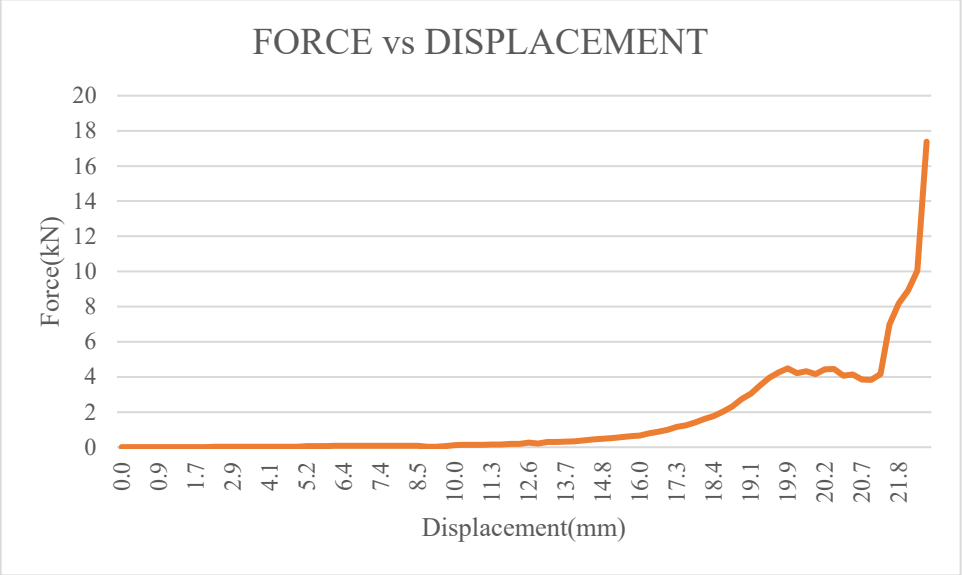

Figure 64. Static Experimental Force vs Displacement curve of Multi-material t-2mm and l-3mm

6.6.9 Cell wall thickness 2 and cell size 3.5

From the figure 65 we can observe that the material experiences a progressive failure. During compression the material reaches a force of 1.38kN and it produces a kink and then the force reaches up to 1.9kN with another kink and finally reaches 2.1kN and increases steeply indicating the inability of the material to absorb further force or energy, which is due to the stiffness of the material.

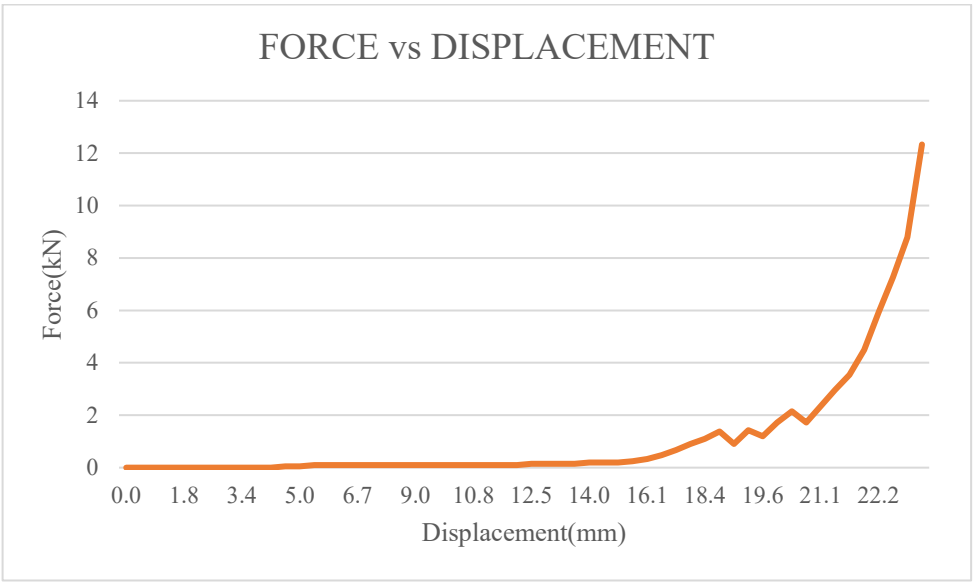

Figure 65. Static Experimental Force vs Displacement curve of Multi-material t-2mm and l-3.5mm

Table 3: Comparison of analytical and experimental static testing values of single and multi-material honeycomb structure

MODEL	ANALYTICAL FORCE (kN)	EXPERIMENTATION FORCE (kN)
SINGLE MATERIAL T1, L2.5	4.5	4.9
MULTI-MATERIAL T1, L2.5	5	3.4
SINGLE MATERIAL T1, L3	4	4.75
MULTI-MATERIAL T1, L3	3	2.1
SINGLE MATERIAL T1, L3.5	5	4.45
MULTI-MATERIAL T1, L3.5	2.1	0.9
SINGLE MATERIAL T1.5, L2.5	10	9.89
MULTI-MATERIAL T1.5, L2.5	3	4.34
SINGLE MATERIAL T1.5, L3	9.9	9.58
MULTI-MATERIAL T1.5, L3	1.5	3.6
SINGLE MATERIAL T1.5, L3.5	7.5	7.4
MULTI-MATERIAL T1.5, L3.5	0.9	1.14
SINGLE MATERIAL T2, L2.5	15	14.5
MULTI-MATERIAL T2, L2.5	7.5	6.26
SINGLE MATERIAL T2, L3	12.5	12
MULTI-MATERIAL T2, L3	4	4.47
SINGLE MATERIAL T2, L3.5	12	11.5
MULTI-MATERIAL T2, L3.5	1.25	1.38

For a better comparison of the experimental and analytical static behaviour of additive manufactured single and multi-material honeycomb structures is presented in the form of a bar chart as shown in the figure 66 below.

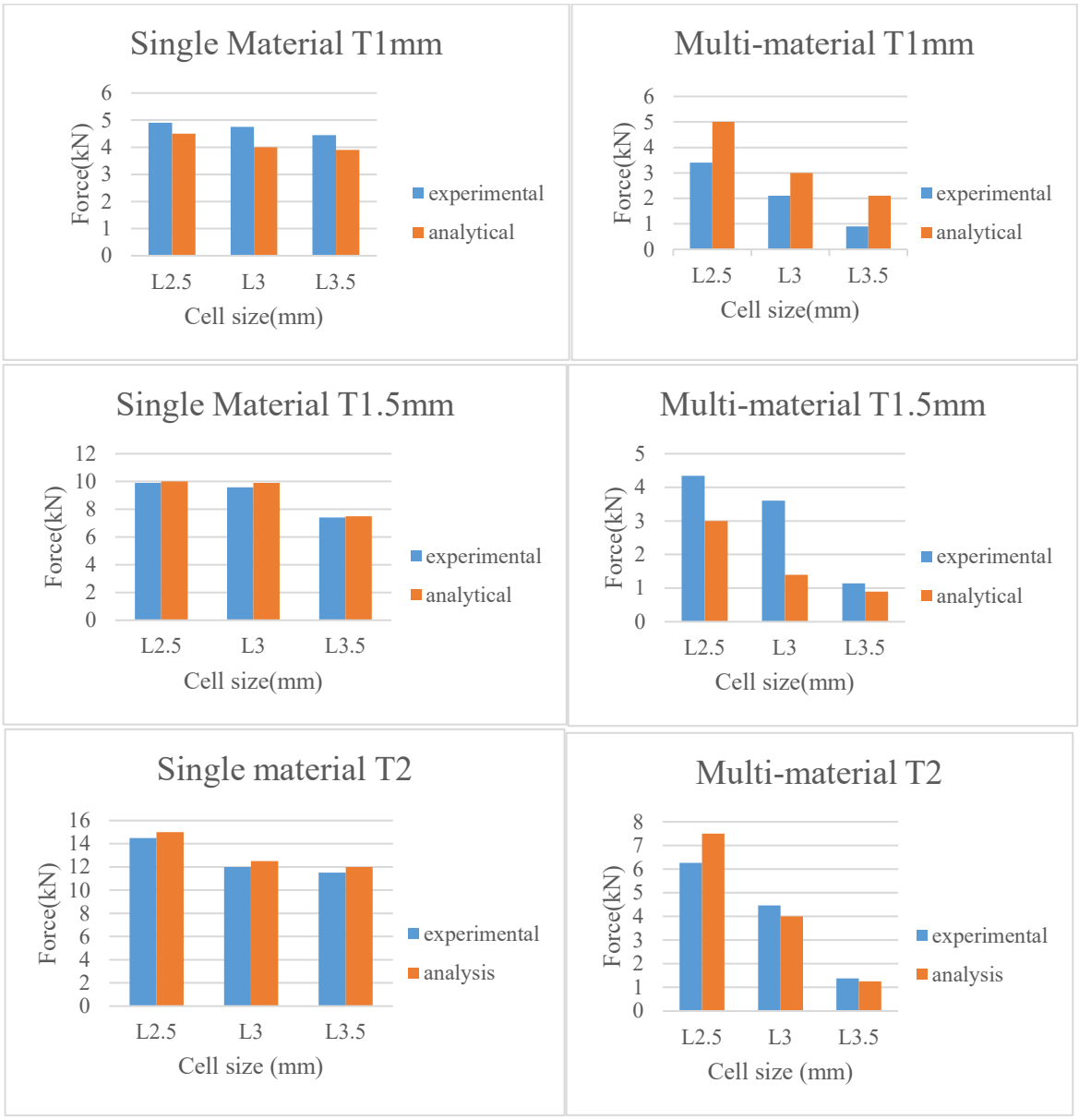

Figure 66. Comparison of experimental and analytical Static behaviour of single and multi-material honeycomb structures

It is evident from the above results that the multi-material absorbs more energy compared to the single material, both of these material tend to fail due to failure during buckling. In the case of single material failure occurs in the mid-section but due to the intricate honeycomb shapes makes the structure more stiff which does not allow the whole structure to buckle outwards. These intricate stiff honeycomb structures resists the buckling outwards, due to which the material fails at the mid-section buckling in the inward direction as shown in figure 67 and figure 68, this shows that there is compressive stress in the outer surface of the honeycomb and tensile stress on the inner surface of the honeycomb structure. This behaviour of compressive stress on the outer surface and tensile stress on the inner surface is due to the material density which holds the whole structure together and induces more stress inwards. Since the buckling is inward the

intricate honeycomb structures get detached during compression from the top surface but the bottom surface of the honeycomb are intact. This is not the same in the multi-material, as seen from the figure 65 the buckling occurs uniformly outwards in the elastomer region and slides away the mid stiff material laterally to a certain extent as figure 65. In this case compressive stress is observed in the inner surface tensile stress on the outer surface of the elastomer. This behaviour of compressive stress on the inner surface and tensile stress on the outer surface is due to the low density of the material which allows the elastomer to buckle outwards as shown in figure 66.

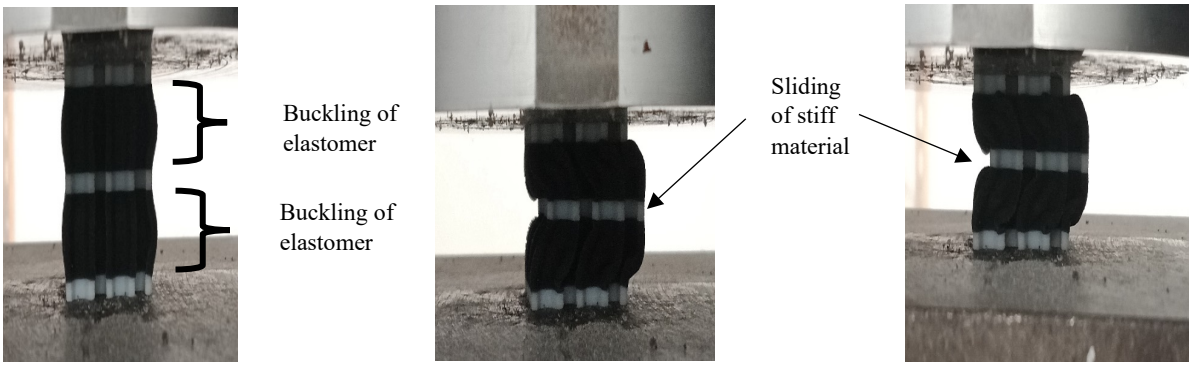

(a)

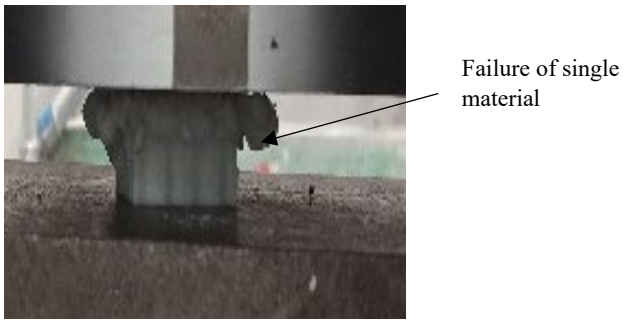

(b)

Figure 67. Compression testing of single and multi-material honeycomb structure

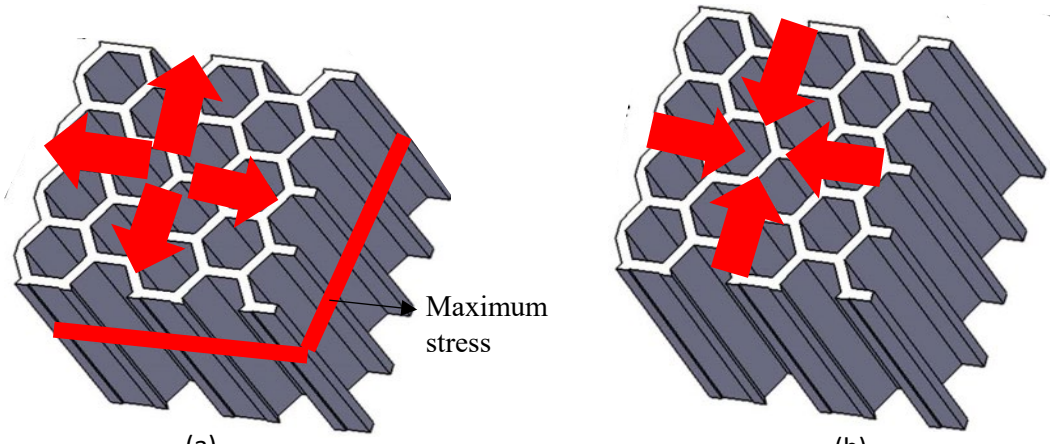

Figure 68. Stress Distribution in (a) single material and (b) Multi-Material

6.7 EFFECT OF CELL WALL THICHKNESS IN MULTI-MATERIAL

As the present study involves variations in the cell wall thickness, the effect of cell wall thickness does have an impact on energy absorption irrespective of the cell wall size. It is observed from the figure 69 that the minimum cell wall thickness with 1mm seems to exhibits less force compared to the other cell wall thickness. This shows the tendency of the material to buckle which is evident from the theoretical model equation wherein the thickness is in the numerator and the cell wall size in the denominator. This shows that increase in cell wall thickness is directly proportional to the force or stress induced i.e. the increase in cell wall thickness increases the stress or force induced.

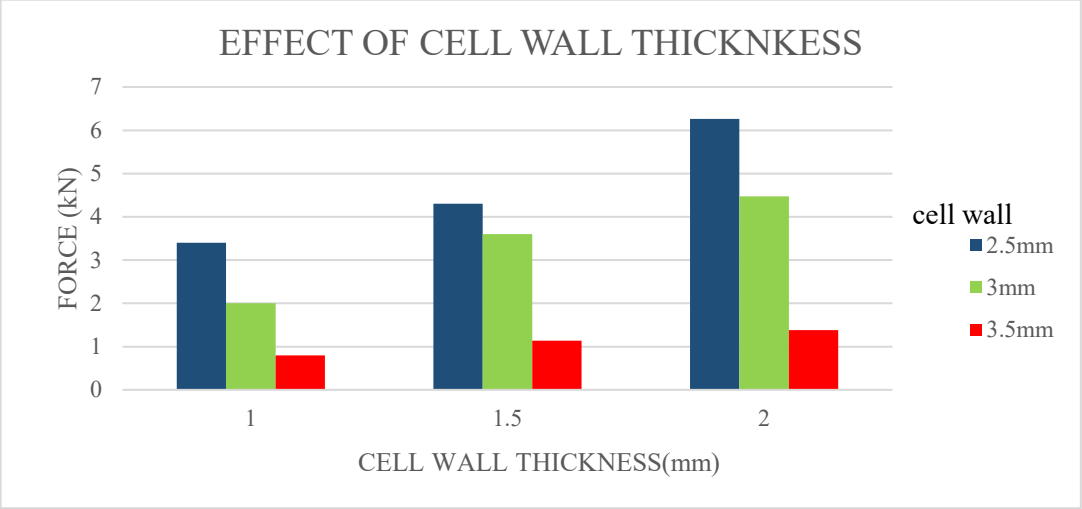

Figure 69. Effect of Cell wall thickness of Multi-Material honeycomb structure

6.8 EFFECT OF CELL SIZE IN MULTI-MATERIAL

It is observed that variations in the cell wall size does have an impact on energy absorption irrespective of the cell wall thickness. From figure 70 the minimum cell wall size with 2.5mm exhibits maximum force compared to the other cell wall size. This shows the tendency of the material to buckle as can be understood from the theoretical model equation, wherein the cell wall thickness is in the numerator and the cell wall size in the denominator. It is understood that the increase in cell wall size is inversely proportional to the force or stress induced i.e. the increase in cell wall size decreases the stress or force induced. This is due to the slenderness ratio induced which allows the material to buckle and take more load.

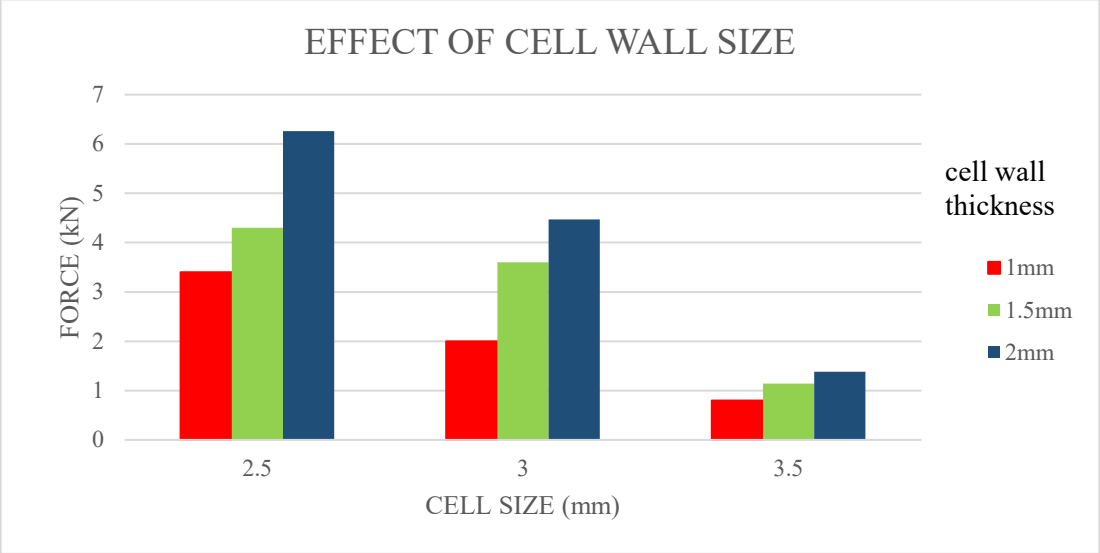

Figure 70. Effect of Cell wall size of Multi-Material honeycomb structure

CHAPTER 7
CONCLUSION

7.1 Conclusion based on Dynamic FEA analysis

Based on the results from the dynamic FEA analysis for single and multi-material based on force vs time the following conclusions are made

- The multi-material honeycomb structure achieves a progressive failure and absorbs more energy compared to single material.
- As the cell wall thickness increases the force experienced by both single and multi-material structure increases due to the stiffness of the whole honeycomb structure.
- As the cell size increases the force experienced by both single and multi-material structure decreases.

7.2 Conclusion based on Static FEA analysis

Based on the results from the static FEA analysis for single and multi-material based on force vs displacement the following conclusions are made

- The multi-material honeycomb structure achieves a progressive failure and absorbs more energy compared to single material.
- As the cell wall thickness increases the force experienced by both single and multi-material structure increases due to the stiffness of the whole honeycomb structure.
- As the cell size increases the force experienced by both single and multi-material structure decreases.

7.3 Conclusion based on Static Experimental Results

Based on the static experimental results for single and multi-material based on force vs displacement the following conclusions are made

- The multi-material honeycomb structure achieves a progressive failure and absorbs more energy compared to single material.
- For cell wall thickness of 1mm in multi-material the force experienced by cell size of 3.5mm is 82.3% lower than the cell size of 2.5mm.
- For cell wall thickness of 1mm in multi-material the force experienced by cell size of 3mm is 55.6% lower than the cell size of 2.5mm.
- For cell wall thickness of 1mm in multi-material the force experienced by cell size of 2.5mm is maximum.
- For cell wall thickness of 1.5 mm in multi-material the force experienced by cell size of 3.5mm is 77.8% lower than the cell size of 2.5mm.
- For cell wall thickness of 1.5 mm in multi-material the force experienced by cell size of 3mm is 28% lower than the cell size of 2.5mm.

- For cell wall thickness of 1.5 mm in multi-material the force experienced by cell size of 2.5mm is maximum.
- For cell wall thickness of 2 mm in multi-material the force experienced by cell size of 3.5mm is 77.6% lower than the cell size of 2.5mm.
- For cell wall thickness of 2 mm in multi-material the force experienced by cell size of 3mm is 28.6% lower than the cell size of 2.5mm.
- For cell wall thickness of 2 mm in multi-material the force experienced by cell size of 2.5mm is maximum.

The analytical results are also experimentally validated and it has been concluded that, as the cell size increases the force experienced by both single and multi-material structure decreases. As the cell wall thickness increases the force experienced by both single and multi-material structure increases due to the stiffness of the whole honeycomb structure. From the conclusion it is evident that the experimental results are in liaise with the theoretical equation where the thickness of the cell wall increases the force or stress induced increases and if the cell size increases the force or stress induced decreases.

REFERENCES

A.T. Beyene, E.G.Koricho, G.Belingardi & B.Martorana, *"Design and manufacturing issues in the development of light weight solution for a vehicle frontal bumper"*, International Symposium on Dynamic Response and Failure of Composite Materials, DRaF2014.

ASTM. "ASTM F2792-10 Standard Terminology for Additive Manufacturing Technologies." American Society for Testing and Materials (ASTM).

B. Hou, H. Zhao, S. Pattofatto , J.G. Liu & Y.L. Li , *"Inertia effects on the progressive crushing of aluminium honeycombs under impact loading",* International Journal of Solids and Structures 49 (2012) 2754–2762.

Bae-Young Kim, Choong-Min Jeong, Si-Woo Kim and Myung-Won Suh, *"A study to maximize the crash energy absorption efficiency within the limits of crash space"*, Journal of Mechanical Science and Technology 26 (4) (2012) 1073~1078.

Cesar A. Terrazas, Sara M. Gaytan, Emmanuel Rodriguez, David Espalin, Lawrence E. Murr, Francisco Medina, Ryan B. Wicker *"Multi-material metallic structure fabrication using electron beam melting"* International Journal of Advanced Manufacturing and Technology(2014)71:33-45.

D. Dutta, F.B. Prinz, D. Rosen, and L. Weiss, *"Layered Manufacturing: Current Status and Future Trends"*, J. Comput. Inform. Sci. in Eng., (ASME), Vol 1_Issue 1, pp. 60-71, 2001.

Dahai Zhang, Qingguo Fei, Jingze Liu, Dong Jian & Yanbin Li, *"Crushing of vertex-based hierarchical honeycombs with triangular substructures"*, Thin-Walled Structures 146 (2019).

Elza Thomas Ukken, Beena B.R *"Review on structural performance of honeycomb sandwich panel"* International Research Journal of Engineering and Technology-04(06)2017, 2558-2562.

F. N. Habib, P. Iovenitti, S. H. Masood & M. Nikzad, *"Cell geometry effect on in-plane energy absorption of periodic honeycomb structures",* International Journal of Advanced Manufacturing Technology (2018) 94:2369–2380, DOI 10.1007/s00170-017-1037-z.

Frank Cooper, Sintering and additive manufacturing: ''additive manufacturing and the new paradigm for the jewellery manufacturer'' Springer, Progress in Additive Manufacturing (2016) 1:29–43.

G. Brett Compton and A. Jennifer Lewis. *"3D-Printing of Lightweight Cellular Composites"*, Advanced Materials 2014, 26(34):5930-5.

H. Zhao, I. Elnasri & S. Abdennadher, *"An experimental study on the behaviour under impact loading of metallic cellular materials",* International Journal of Mechanical Sciences 47 (2005) 757–774.

Han Zhao and Gerard Gary, "*Crushing behaviour of aluminium honeycombs under impact loading",* Int. J. Impact Engng Vol. 21, No. 10, pp. 827D836, 1998, PII: S0734-743X(98)00034-7.

Houria Salem, Djilali Boutchicha & Abdelmadjid Boudjemai *"Modal analysis of the multi-shaped coupled honeycomb structures",* International Journal on Interactive Design and Manufacturing (IJIDeM) 2017.

I.Gibson, D.W. Rosen and B. Stucker "*Additive Manufacturing Methodologies: Rapid Prototyping to Direct Digital Manufacturing",* Springer 2010.

J Zhang, M.F. Ashby, *"The out-of-plane properties of honeycomb"*, International Journal of Mechanical Sciences, vol. 34, No. 6, pp:475-489, 1992.

Kaufui V.Wong and Aldo Hernandez, Review Article: A Review of Additive Manufacturing, International Scholarly Research Network ISRN Mechanical Engineering Volume 2012, Article ID 208760, 10 pages doi:10.5402/2012/208760.

Konstantinos Salonitis, "Design for additive manufacturing based on the axiomatic design method" Springer, International Journal of Advanced Manufacturing Technology (2016) 87:989–996.

Kun Sun, Dichen Li, Haihua Wu, Minjie Wang, Xiaoyong Tian, (2012) "Three-dimensional multi-material electromagnetic band-gap structure: design, fabrication and property studies", Rapid Prototyping Journal, Vol. 18 Issue: 3, pp.222-229.

M. Sugavaneswaren and G. Arumaikkannu."*Modelling for randomly oriented multi material additive manufacturing component and its fabrication*", Materials & design, vol 54, pp.779-785, 2014.

Mohammad Vaezi, Srisit Chianrabutra, Brian Mellor & Shoufeng Yang (2013), *"Multiple material additive manufacturing-Part 1: a review"*, Virtual and Physical Prototyping, 8:1, 19-50.

Quirino Estrada & Dariusz Szwedowicz & Martin Baltazar & Claudia Cortes & Tadeusz Majewski & Claudio A. Estrada "*The performance of energy absorption in structural profiles*" International Journal of Advanced Manufacturing Technologies (2016) 84:1081–1094.

S. Kumar and J.P. Kruth."Composites by Rapid Prototyping Technology", *Materials and Design,* Vol.31, JP 2010.

S. Slimane, S. Kebdani, A. Boudjemai & A. Slimane, *"Effect of position of tension-loaded inserts on honeycomb panels used for space applications",* International Journal of Interactive Design for Manufacturing, DOI 10.1007/s12008-017-0383-2.

Tejasagar Ambati, K.V.N.S. Srikanth & P. Veeraraju *"Simulation of vehicular frontal crash test"* International Journal of Applied Research in Mechanical Engineering (IJARME) ISSN: 2231 –5950, Volume-2, Issue-1, 2012.

Vijayanand Rajendra Boopathy, Anantharaman Sriraman, Arumaikkannu G., *"Energy absorbing capability of additive manufactured multi-material honeycomb structure"*, Rapid Prototyping Journal (2019), 25 (3), 623-629.

Vincent Caccese, James R. Ferguson, Michael A. Edgecomb, *"Optimal design of honeycomb material used to mitigate head impact"*, Composite Structures 100(2013), 404-412.

W. E. Baker, T. C. Togami and J. C. Weydert, *"Static and dynamic properties of high-density metal honeycombs",* Int. J. Impact Engng Vol. 21, No. 3, pp. 149Ð163, 1998 PII: S0734±743X(97)00040±7.

Y. Liu and I. Gibson, "A framework for development of a fibre-composite, curved FDM system". *Proceedings of the International Conference on Manufacturing Automation, ICMA'07,* 28–30 May, Singapore, pp. 93–102, 2007.

Yeong-Eun Lim, Na-Hyun Kim, Hye-Jin Choi & Keun Park, *"Design for additive manufacturing of customized cast with porous shell structures"*, Journal of Mechanical Science and Technology 31 (11) (2017) 5477~5483, DOI 10.1007/s12206-017-1042-z.

Yong-Jin Yoon, Seung Ki Moon, and Jihong Hwang *"3D printing as an efficient way for comparative study of biomimetic structures trabecular bone and honeycomb"* Journal of Mechanical Science and Technology 28 (11) (2014) 4635-4640 DOI 10.1007/s12206-014-1031-4.

Zhao Liu, Jiahai Lu, Ping Zhu, *"Lightweight design of automotive composite bumper system using modified particle swarm optimizer"*, Composite Structures 140 (2016) 630–643.